1971

The crystal structure determinations of rubidium hexabromoantimonate(III,V) and tetramethylammonium nonabromodiantimonate(III) dibromine and a highly efficient white radiation neutron diffraction technique

Camden Richards Hubbard
Iowa State University

Recommended Citation

Hubbard, Camden Richards, "The crystal structure determinations of rubidium hexabromoantimonate(III,V) and tetramethylammonium nonabromodiantimonate(III) dibromine and a highly efficient white radiation neutron diffraction technique " (1971). *Retrospective Theses and Dissertations*. 4462.
https://lib.dr.iastate.edu/rtd/4462

72-5210

HUBBARD, Camden Richards, 1944-
THE CRYSTAL STRUCTURE DETERMINATIONS OF RUBIDIUM HEXABROMOANTIMONATE (III,V) AND TETRAMETHYLAMMONIUM NONABROMODIANTIMONATE(III) DIBROMINE AND A HIGHLY EFFICIENT WHITE RADIATION NEUTRON DIFFRACTION TECHNIQUE.

Iowa State University, Ph.D., 1971
Chemistry, physical

University Microfilms, A XEROX Company, Ann Arbor, Michigan

The crystal structure determinations of rubidium hexabromoantimonate(III,V) and tetramethylammonium nonabromodiantimonate(III) dibromine and a highly efficient white radiation neutron diffraction technique

Camden Richards Hubbard

A Dissertation Submitted to the
Graduate Faculty in Partial Fulfillment of
The Requirements for the Degree of
DOCTOR OF PHILOSOPHY

Major Subject: Physical Chemistry

Approved:

Signature was redacted for privacy.

In Charge of Major Work

Signature was redacted for privacy.

For the Major Department

Signature was redacted for privacy.

For the Graduate College

Iowa State University
Ames, Iowa

1971

TABLE OF CONTENTS

INTRODUCTION

The research described in this thesis encompasses four areas of concentration in the broad field of crystallography. The crystal structures of rubidium hexabromoantimonate(III,V) and tetramethylammonium nonabromodiantimonate(III) dibromine were determined by three dimensional X-ray analysis to elucidate the molecular bonding and other physical properties of these compounds. The rubidium salt was found to contain ordered $Sb^{III}Br_6$ and $Sb^{V}Br_6$ octahedra. Unusual bridging of $Sb_2{}^{III}Br_9$ anions by molecular bromine was found in the tetramethylammonium salt.

A neutron diffraction technique using a polychromatic beam was developed. This technique dramatically increases both counting precision and data collection rates over conventional monochromatic beam techniques. Data collected from an α-oxalic acid dihydrate crystal was used to test the method. Refinement based on all the observed intensities produced parameters which are in excellent agreement with literature values.

A new method to solve the phase problem was proposed and tested. This method couples Patterson deconvolution and direct methods thru use of Fourier coefficients calculated from a superposition map. This method incorporates the advantages of both Patterson deconvolution and direct methods. Three known structures were solved using this method.

To aid in this research numerous computer programs were written. The system of programs for generalized superpositions and the Fourier programs employing the fast Fourier algorithm provide some of the necessary computer calculations required during a crystal structure determination. These programs also provide great flexibility for studying direct-space reciprocal-space methods of crystal structure determination.

THE CRYSTAL STRUCTURE OF RUBIDIUM HEXABROMOANTIMONATE(III,V)

Introduction

Antimony halide compounds have been under investigation for many years. Of primary interest have been halide salts of the mixed valence type, $M^{III} - Sb^{V}$, ($M = Sb^{III}$, Bi^{III}, In^{III}, Tl^{III}).[1,2] These salts are abnormally dark in color indicating a strong absorption of visible light. This was reported to be due to an electron transfer from the $M^{III}X_6{}^{3-}$ ion to the $Sb^{V}X_6{}^{-}$ ion via van der Waals contacts through the halogens and/or the cations.[2-4] Examples of the mixed valence state compounds are $(NH_4)_4Sb^{III}Sb^{V}Br_{12}$,[1] $Cs_4Bi^{III}Sb^{V}Cl_{12}$[2] and $(C_5H_5NH)_6Sb^{III}Sb_3{}^{V}Br_{24}$.[3] However, it is possible in some cases to obtain dark antimony salts containing antimony in only one oxidation state; for example, the structure of $(C_6H_7NH)_2SbBr_9$[4] has been recently determined and was found to contain $Sb^{V}Br_6{}^{-}$ and $Br_3{}^{-}$ groups. A review of many of the physical properties of these antimony compounds such as diffuse reflectance spectra, density, melting point, color dependence on temperature, crystal class, method of preparation, etc., is given by Hackert et al.[5]

If the proposed charge transfer is to be further investigated, then more structural information on related compounds is needed. An understanding of the effects of packing, bond distances and angles, change of cation, change of halide, etc., will be necessary for complete characterization of these unusual antimony halide compounds.

The configuration of the bromine atoms about the Sb^{III} atom is also of considerable interest since antimony(III) is of $d^{10}s^{2}$ configuration. In the $(NH_4)_4Sb^{III}Sb^{V}Br_{12}$ structure, Lawton found that the $Sb^{III}Br_6{}^{3-}$ ion had O_h symmetry while the $Sb^{V}Br_6{}^{-}$ ion of $d^{10}s^{0}$ configuration had D_{2d} symmetry.

Rubidium also forms a salt with empirical formula Rb_2SbBr_6 which is black in color. It was decided to carry out a single crystal structural investigation of this compound to determine whether it is essentially isomorphous with the ammonium salt, and if so, what effect the spherically symmetric cation would have on the structure in general and on the symmetry of the $SbBr_6$ groups.

Experimental

Rb_2SbBr_6 was prepared by the method of Hackert et al.[5], a modification of the method of Ephraim and Weinberg.[6] The jet black octahedral crystals were crystallized from conc. HBr (48%). Because the crystals were reported to decompose slowly in air, they were placed in thin-walled, Lindemann glass capillaries.

Preliminary investigation using precession and Weisenberg photographs showed that the unit cell is tetragonal with space group $I4_1/amd$. The unit cell parameters at room temperature are $\underline{a} = 10.706 \pm 0.003$ and $\underline{c} = 21.695 \pm 0.022$ Å. These parameters and their standard deviations were obtained from measurements on a General Electric single crystal orienter using Cr K_α radiation for 16 reflections in the two theta range 45-118° and agree quite well with those reported by Jensen and Rasmussen.[7] The refinement of the lattice constants was carried out using a program of Williams which employs the Nelson-Riley extrapolation function.[8]

In the ammonium salt $\underline{a}$ = 10.66, $\underline{c}$ = 21.52 Å, and the space group is $I4_1/amd$. Therefore the assumption that the rubidium salt was nearly isomorphic with the ammonium salt seemed quite reasonable. On this basis a calculated density of 4.17 g/cc was obtained assuming eight Rb_2SbBr_6 formula units/unit cell.

Using zirconium-filtered molybdenum radiation, X-ray intensity data were collected at room temperature from an octahedral crystal of dimensions 0.28 × 0.28 × 0.30 mm (μ = 296 cm^{-1}). A General Electric single crystal orienter equipped with a scintillation counter was used employing the peak height measurement technique. The single crystal orienter settings were precalculated by a program of Williams.[9] Only those reflections noticeably above background were measured in the molybdenum radiation sphere of radius $\sin \theta/\lambda = 0.705$ ($2\theta = 60°$). A total of 473 independent reflections were observed.

The raw intensities for all reflections were converted from peak height data to integrated intensities using the method of Alexander and Smith.[10] This conversion also included a correction for $K\alpha_1 - K\alpha_2$ splitting. The integrated intensity data were then corrected for background, absorption, decomposition, Lorentz-polarization, and non-characteristic radiation streaking. The background correction was obtained from plots of averaged background versus 2θ for two different phi values to adjust for the small dependence of background with phi. The streak correction was based on the method of Williams and Rundle.[11] The individual transmission factors were calculated using the program of Wehe, Busing and Levy.[12] Three standard reflections were observed periodically and indicated a slight decomposition of the crystal during the experiment.

Solution and Refinement

The structure was solved without reference to the ammonium salt. A Patterson map was generated and all atoms were located. From the crystallographic positions of space group $I4_1/amd$ and the positions determined from the Patterson map, the eight antimony atoms must be distributed in two different crystallographic positions, four in position a, and four in position b. The two types were assumed to be antimony (V) and antimony(III). Antimony(V) was arbitrarily assigned to position a.

A modification of the full-matrix least-squares program of Busing, Martin and Levy[13] was used to refine the structure with the center of symmetry at the origin. Hartree-Fock-Slater atomic scattering factors[14] were used for antimony, rubidium, and bromine with corrections for the real and imaginary contributions to anomalous dispersion.[15] The seven atoms were refined isotropically to an unweighted discrepancy index, $R = \Sigma||F_o|-|F_c||/\Sigma|F_o| = 0.190$. Considerable anisotropic motion was observed for the bromines on an electron density map. The structure was then refined anisotropically to $R = 0.134$.

At this point all the reflections were carefully examined for any which may have been measured incorrectly. The four largest reflections were in very poor agreement, $|F_c|-|F_o| \geq 9\sigma$. They seemed to be suffering from extinction and were removed from the data set. An additional 41 very weak reflections for which $F_o < 2\sigma$ were also removed.[16] Another 27 weak reflections for which $||F_o|-|F_c|| \geq 2|F_o|$ or $2|F_c|$ were removed as it was felt that these were measured incorrectly. The weighting scheme was then improved by plotting $\overline{\omega\Delta^2}$ for ten overlapping groups of about 80 reflections each versus F_o $[\Delta^2 = (|F_o|-|F_c|)^2$ and $\omega = (1/\sigma^2)]$. The equation of the above curve was then used to derive an improved set of weights such that $\overline{\omega\Delta^2}$ was nearly constant.

The structure was refined for four additional cycles using the remaining 401 reflections (∿13 reflections per variable). The average shift in bond length was about 0.01 Å, and the average decrease in the standard deviation as calculated by

ORFFE[17] was about 50%. Thus the removal of this data found to be in very poor agreement seems to be justified.

The final discrepancy indexes are listed in Table 1 for all data, for ℓ-even only and for ℓ-odd only. The ℓ-odd reflections would be systematically extinct if both $SbBr_6$ groups were identical. Hence the ℓ-odd reflections arise from the differences between the $Sb^{V}Br_6{}^{-}$ and the $Sb^{III}Br_6{}^{3-}$ groups. Figure 1 shows the unit cell and the arrangement of the $Sb^{V}Br_6{}^{-}$ and $Sb^{III}Br_6{}^{3-}$ octahedra.

Table 1. Discrepancy indexes

Type of F_{obs} data	No. of reflections	Unweighted R	Weighted R
$hk\ell$:all data	401	0.102	0.084
$hk\ell$:ℓ-even only	235	0.090	---
$hk\ell$:ℓ-odd only	166	0.131	---

Table 2 lists the final atomic parameters (origin at $\bar{4}m2$, 0, -1/4, 1/8 from the origin used in the refinement). These positions correspond to the same orientation as in Figure 2. The computer drawings shown throughout the text were made using ORTEP.[18] Table 3 lists the observed and calculated structure factors.

Figure 1. The unit cell of tetragonal $Rb_4Sb^{III}Sb^{V}Br_{12}$ showing the alternation of Sb^{V} (small black circles) and Sb^{III} (small white circles) along the c-axis. Each antimony atom is positioned at the center of an octahedron formed by six bromine atoms. Rubidium atoms are represented by the large white circles. Distortions of the anions are not shown

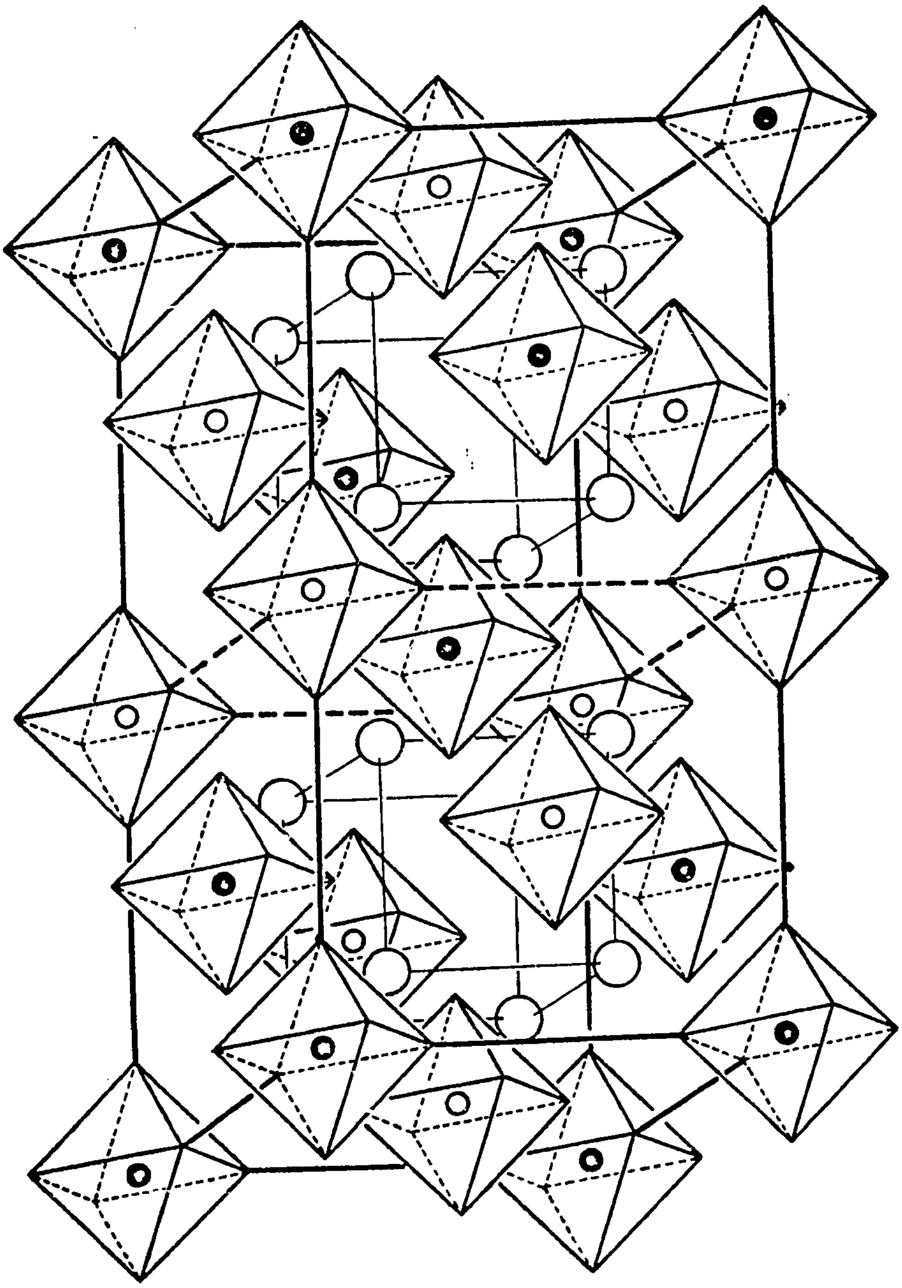

Table 2. Final atomic parameters[a] (Errors in least significant figures in parentheses)

Atom	Pos.	x[b]	y	z	β_{11}[c]	β_{22}	β_{33}	β_{12}	β_{13}	β_{23}
Sb^{V}	4a	0	1/2	1/4	45(5)	β_{11}	20(1)	0	0	0
Sb^{III}	4b	0	0	1/2	52(6)	β_{11}	16(1)	0	0	0
Br_1	16h	0	0.26477(5)	0.25260(3)	183(7)	62(4)	55(2)	0	0	-21(3)
Br_2	16h	0	0.25970(3)	0.49731(2)	90(4)	45(3)	22(1)	0	0	-13(2)
Br_3	8e	0	1/2	0.37013(4)	195(18)	β_{11}	48(3)	0	0	0
Br_4	8e	0	0	0.37502(2)	59(6)	β_{11}	12(1)	0	0	0
Rb	16f	1/4	0.22294(47)	3/8	104(6)	91(5)	32(1)	0	3.6(1.6)	0

[a] Origin at $\bar{4}m2$.

[b] Fractional unit all coordinates.

[c] β's × 10^4; the anisotropic temperature factor expression is $\exp-(\beta_{11}h^2+\beta_{22}k^2+\beta_{33}\ell^2+2\beta_{12}hk+2\beta_{13}h\ell+2\beta_{23}k\ell)$.

Figure 2. A portion of the unit cell of $Rb_4Sb^{III}Sb^{V}Br_{12}$ showing the rubidium ions with respect to the relative distribution of distorted $Sb^{V}Br_6^{-}$ and $Sb^{III}Br_6^{3-}$ ions. The b-axis is across the page, c vertical, and a into the page

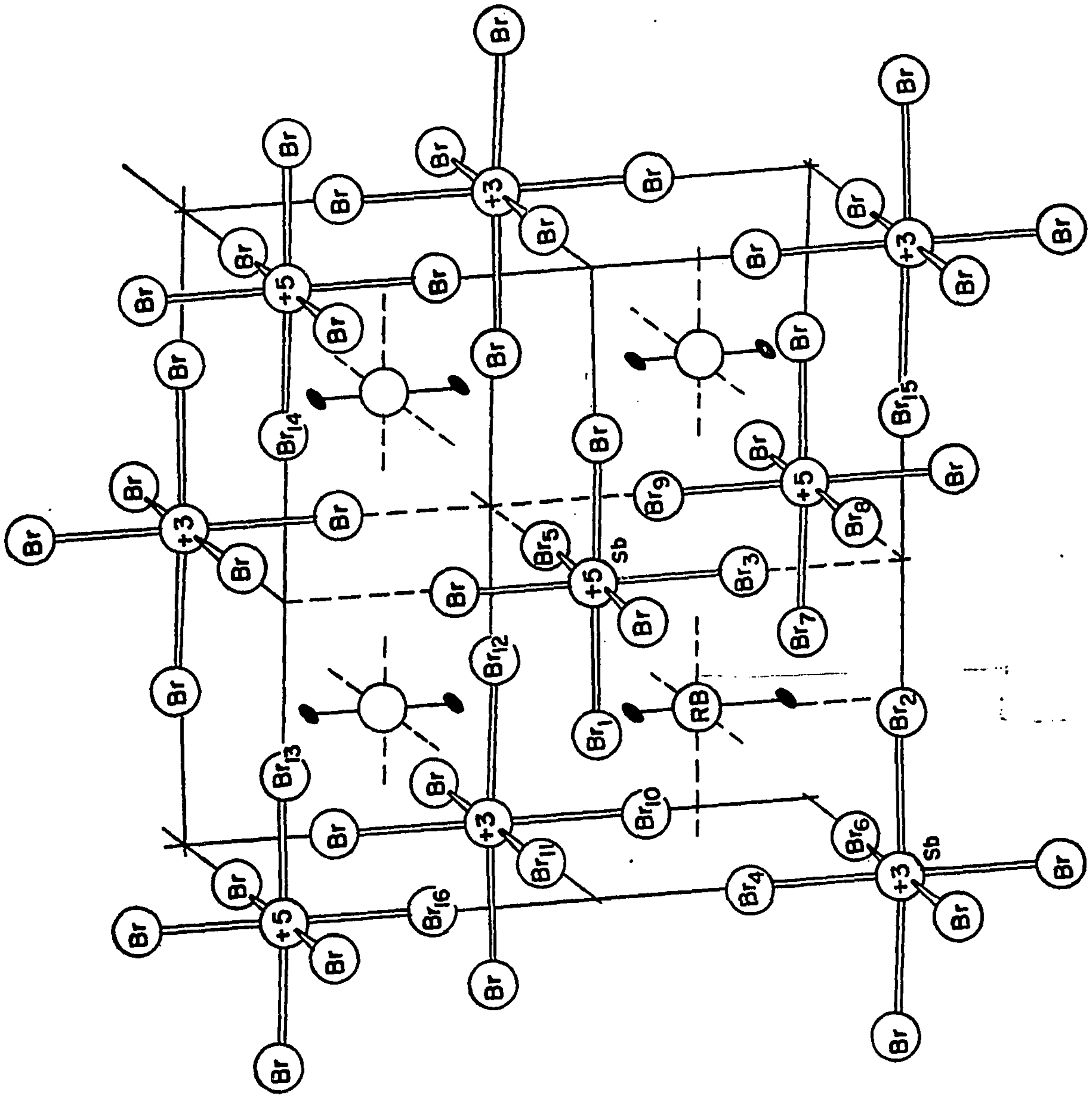
Br
+3
+5
Sb
RB
Br1
Br2
Br3
Br4
Br5
Br6
Br7
Br8
Br9
Br10
Br11
Br12
Br13
Br14
Br15
Br16

Table 3. List of F_o and F_c

```
K= 0,L= 0
H F(O) F(C)
21157  712
81605 1644
10 578  619

K= 0,L= 1
H F(O) F(C)
 9 109  151
15 109  118

K= 1,L= 1
H F(O) F(C)
 2 150  137

K= 2,L= 1
H F(O) F(C)
 3 389  339
 5 377  415
 7 342  387
 9 291  308
11 199  226
13 132  144

K= 3,L= 1
H F(O) F(C)
 6 199  206

K= 4,L= 1
H F(O) F(C)
 5 113  103

K= 5,L= 1
H F(O) F(C)
 6 220  237

K= 6,L= 1
H F(O) F(C)
 7 229  243
 9 166  192
11  98  143

K= 0,L= 2
H F(O) F(C)
 4 118   90
 8 184  160
10 131  118
12 120   95

K= 1,L= 2
H F(O) F(C)
 3 707  653
 5 585  594
 7 399  387
 9 320  335
11 160  214
13 148  192
15  78  117

K= 2,L= 2
H F(O) F(C)
 6 120  124
 8 108  163

K= 3,L= 2
H F(O) F(C)
 3 499  556
 5 437  522
 7 349  378
 9 303  316
11 162  219
13 124  148

K= 5,L= 2
H F(O) F(C)
 5 403  439
 7 306  330
 9 235  238
11 144  186

K= 7,L= 2
H F(O) F(C)
 7 249  193
 9 182  213
11 123  193

K= 0,L= 3
H F(O) F(C)
 1 162  181
 3 381  337
 5 450  438
 7 371  381
 9 307  328
11 218  205
13 150  160

K= 1,L= 3
H F(O) F(C)
 4 101  139
 8  86   93

K= 2,L= 3
H F(O) F(C)
 3 176  168
 7 132  165

K= 3,L= 3
H F(O) F(C)
 4 211  224
 6 143  171

K= 4,L= 3
H F(O) F(C)
 5 302  345
 7 275  285
 9 243  261

11 128  157
13 116  128

K= 5,L= 3
H F(O) F(C)
 6 104  107

K= 6,L= 3
H F(O) F(C)
 9 130  141

K= 0,L= 4
H F(O) F(C)
 0 870  683
 2 731  676
 4 618  618
 6 315  301
 8 483  469
10 108   78
12 260  250

K= 2,L= 4
H F(O) F(C)
 4 547  545
61305 1305
 8 326  317
10 362  424
12 135  149

K= 4,L= 4
H F(O) F(C)
 4 513  575
 6 241  253
 8 451  427
12 246  227

K= 6,L= 4
H F(O) F(C)
 6 702  709
 8 151  160
10 201  228

K= 8,L= 4
H F(O) F(C)
 8 347  307
12 177  166

K= 0,L= 5
H F(O) F(C)
 1 192   93
 3 330  346
 5 389  387
 7 402  369
 9 331  319
11 233  205
13 159  170

K= 1,L= 5
H F(O) F(C)
 4 102   81
 6 126   95

K= 2,L= 5
H F(O) F(C)
 5 135   62

K= 3,L= 5
H F(O) F(C)
 4 203  247

K= 4,L= 5
H F(O) F(C)
 5 285  305
 7 276  286
 9 240  257
11 143  161
13 135  138

K= 5,L= 5
H F(O) F(C)
 8 172  159

K= 7,L= 5
H F(O) F(C)
 8 121  144

K= 8,L= 5
H F(O) F(C)
 9 167  138

K= 0,L= 6
H F(O) F(C)
 2 170  184
 4 110   91
 6 167  223
 8 166  157
10 167  170
12 103  104

K= 1,L= 6
H F(O) F(C)
 1 502  595
 3 501  501
 5 476  476
 7 351  329
 9 306  288
11 169  196
13 161  137

K= 2,L= 6
H F(O) F(C)
 4 100   66
10 132   93

K= 3,L= 6
H F(O) F(C)
 5 420  420
 7 331  329
 9 160  268
11 175  205
13 107  131

K= 4,L= 6
H F(O) F(C)
 6  80  130

K= 5,L= 6
H F(O) F(C)
 5 362  370
 7 285  280
 9 210  214
11 151  167

K= 7,L= 6
H F(O) F(C)
 7 245  275
 9 198  187
11 132  181

K= 0,L= 7
H F(O) F(C)
 1 227  172
 3 102   76
 5 261  232
 7 117  119
 9 141  126
11 120  137

K= 1,L= 7
H F(O) F(C)
 2  60   65
 4 212  180
 8 115  121

K= 2,L= 7
H F(O) F(C)
 3 263  286
 5 304  303
 7 320  309
 9 247  236
11 166  172
13  98  105

K= 3,L= 7
H F(O) F(C)
 4 114   76
 6 185  186

K= 4,L= 7
H F(O) F(C)
 5 203  211

K= 5,L= 7
H F(O) F(C)
 6 183  166
 8 139  151

K= 6,L= 7
H F(O) F(C)
 7 192  198

K= 0,L= 8
H F(O) F(C)
 2 532  540
 6 400  401
81304 1299
10 252  253
12 487  515
14 118  138

K= 1,L= 8
H F(O) F(C)
 3  63   60
 7  94   70

K= 2,L= 8
H F(O) F(C)
 2 546  578
 4 557  562
 6 320  320
 8 481  462
12 270  284

K= 3,L= 8
H F(O) F(C)
 5  96   82

K= 4,L= 8
H F(O) F(C)
42017 2024
 6 421  411
81101 1046
10 221  255
12 432  428
14 113  135

K= 6,L= 8
H F(O) F(C)
 6 169  196
 8 368  360
12 194  227

K= 8,L= 8
H F(O) F(C)
 8 618  583
10 224  223
12 235  269

K= 0,L= 9
H F(O) F(C)
 1 115   96
 3 200   56
 5  81  137

K= 1,L= 9
H F(O) F(C)
 2  93  110
 4 113  129
 6  98   68

K= 2,L= 9
H F(O) F(C)
 3 221  210
 5 315  293
 7 286  287
 9 265  227
11 154  189

K= 3,L= 9
H F(O) F(C)
 4 163   82
 6 165  128

K= 4,L= 9
H F(O) F(C)

K= 5,L= 9
H F(O) F(C)
 6 200  189

K= 6,L= 9
H F(O) F(C)
 7 216  183
 9 168  151
11 110  122

K= 0,L=10
H F(O) F(C)
 2 161  166

K= 1,L=10
H F(O) F(C)
 1 525  589
 3 470  518
 5 440  444
 7 332  331
 9 261  250
11 165  186
13 123  114

K= 2,L=10
H F(O) F(C)
 4 194  187
 6 126   93
 8 172  175
12 138   97

K= 3,L=10
H F(O) F(C)
 3 470  460
 5 424  412
 7 315  312
 9 240  244
11 122  184
13 119  114

K= 5,L=10
H F(O) F(C)
 7 294  276
 9 189  177
11 136  160

K= 6,L=10
H F(O) F(C)
 8 105   76

K= 7,L=10
H F(O) F(C)
 7 250  240
 9 168  176
11 127  154

K= 0,L=11
H F(O) F(C)
 1 118   81
 3 257  180
 5 274  240
 7 216  221
 9 196  186

K= 1,L=11
H F(O) F(C)
 2 159 -153
 4 109   77
 6 146  122

K= 2,L=11
H F(O) F(C)
 3 257  244
 5  99  103
 7 204  201

K= 3,L=11
H F(O) F(C)
 4 146  124
 6 197  188

K= 4,L=11
H F(O) F(C)
 5 212  196
 7 193  165
 9 161  149
13  97   72

K= 5,L=11
H F(O) F(C)
 8 137  113

K= 6,L=11
H F(O) F(C)
 7 160  160

K= 0,L=12
H F(O) F(C)
 2 372  400
 4 324  340
 8 316  287

K= 1,L=12
H F(O) F(C)
 1  60   61
 3  60   61
 7  93   75

K= 2,L=12
H F(O) F(C)
21168 1287
 4 324  336
 6 765  726
 8 224  202
10 248  259
12 141  102

K= 4,L=12
H F(O) F(C)
 4 347  333
 6 186  165
 8 302  268
12 165  154

K= 6,L=12
H F(O) F(C)
 6 285 -417
 8 119  105
10 141  145

K= 8,L=12
H F(O) F(C)
 8 262  202

K= 0,L=13
H F(O) F(C)
 3 216  178
 5 196  211
 7 239  205
 9 198  201
11 167  125
13 105  121

K= 1,L=13
H F(O) F(C)
 2 144   92
 6  91  123

K= 2,L=13
H F(O) F(C)
 3  83  130
 5  84  101

K= 3,L=13
H F(O) F(C)
 4 153  143

K= 4,L=13
H F(O) F(C)
 5 178  170
 7 182  167
 9 161  164
13 112   99

K= 5,L=13
H F(O) F(C)
 8 105   86

K= 8,L=13
H F(O) F(C)
 9 119   89

K= 0,L=14
H F(O) F(C)
 2 178  173
 6 183  173
10 161  118

K= 1,L=14
H F(O) F(C)
 1 278  318
 3 275  296
 5 256  266
 7 238  226
 9 194  170
11 179  146
13 113   85

K= 2,L=14
H F(O) F(C)
 4 105  104

K= 3,L=14
H F(O) F(C)
 3 262  290
 5 266  246
 7 242  232
 9 193  161
11 141  152

K= 4,L=14
H F(O) F(C)
 6 153  114

K= 5,L=14
H F(O) F(C)
 5 263  216
 7 219  183
 9 191  134
11 128  129

K= 7,L=14
H F(O) F(C)
 7 169  195
 9 160  121
11 156  130

K= 0,L=15
H F(O) F(C)
 1 235  246
 3 160  155
 5 237  250
 7 145  106
 9 145  144

K= 1,L=15
H F(O) F(C)
 4 211  208
 8 141  130
12 118   59

K= 2,L=15
H F(O) F(C)
 3 140  120
 5  90  118
 7 154  136
 9 119   92

K= 3,L=15
H F(O) F(C)
 4 156  132
 6 101   85

K= 4,L=15
H F(O) F(C)
 5 235  216
 9 137  127

K= 5,L=15
H F(O) F(C)
 8 155  137

K= 6,L=15
H F(O) F(C)
 7 132   89

K= 0,L=16
H F(O) F(C)
01465 1531
 2 343  339
41194 1235
 6 296  272
 8 738  695
10 187  176
12 303  310

K= 2,L=16
H F(O) F(C)
 2 381  380
 4 338  360
 6 269  239
 8 299  295
10 117  120
12 196  191

K= 4,L=16
H F(O) F(C)
41024 1005
 6 291  272
 8 631  577
10 181  173
12 264  264

K= 5,L=16
H F(O) F(C)
11 102   47

K= 6,L=16
H F(O) F(C)
 6 199  159
 8 277  235

K= 8,L=16
H F(O) F(C)
 8 406  347
10 178  148

K= 0,L=17
H F(O) F(C)
 3 160  116

K= 2,L=17
H F(O) F(C)
 3  73  120
 5 156  103
 7 146  160
11 130  114

K= 3,L=17
H F(O) F(C)
 4 113  117

K= 4,L=17
H F(O) F(C)
11 106   99

K= 5,L=17
H F(O) F(C)
10 107   49

K= 6,L=17
H F(O) F(C)
 7  96  105

K= 0,L=18
H F(O) F(C)
 2 105  115

K= 1,L=18
H F(O) F(C)
 1 314  292
 3 275  276
 5 245  223
 7 218  198
 9 152  129
11 159  121

K= 2,L=18
H F(O) F(C)
 4 120  117
 8 109   95

K= 3,L=18
H F(O) F(C)
 3 155  257
 5 214  219
 7 202  187
 9 108  132
11 149  117

K= 5,L=18
H F(O) F(C)
 5 166  164
 7 177  163
 9 162   95

K= 7,L=18
H F(O) F(C)
 7 161  144
 9 137  103

K= 1,L=19
H F(O) F(C)
 2 173  150
 6 123  112
10 107   63

K= 2,L=19
H F(O) F(C)
 3 176  195
 7 139  156
11 125   73

K= 3,L=19
H F(O) F(C)
 6 129  144
10 135   79

K= 0,L=20
H F(O) F(C)
 2 158  153
 8 126  122

K= 2,L=20
H F(O) F(C)
 2 415  441
 6 252  236
10 110  112

K= 4,L=20
H F(O) F(C)
 8 133  117

K= 6,L=20
H F(O) F(C)
 6 117  169

K= 8,L=20
H F(O) F(C)
 8 117   96

K= 1,L=22
H F(O) F(C)
 5 121  126

K= 3,L=22
H F(O) F(C)
 3  99  158

K= 0,L=23
H F(O) F(C)
 1 133  184
 5 126  190

K= 1,L=23
H F(O) F(C)
 4 115  142

K= 0,L=24
H F(O) F(C)
 0 467  949
 2 152  193
 4 408  461
 8 284  290

K= 2,L=24
H F(O) F(C)
 2 198  193
 4 136  167
 6 147  134
 8 134  158

K= 4,L=24
H F(O) F(C)
 4 366  391
 6 114  150
 8 245  269
```

Description of the Structure

The structure of $Rb_4Sb^{III}Sb^VBr_{12}$ is quite similar to that of the ammonium salt. The existence of weak ℓ-odd reflections indicates that the two $SbBr_6$ groups are indeed different chemical species, presumably $Sb^VBr_6{}^-$ and $Sb^{III}Br_6{}^{3-}$. The antimony-bromine bond lengths in the rubidium salt are noticeably different than in the ammonium salt along the c-axis, but are similar perpendicular to the c-axis. The interatomic distances and angles and their estimated standard deviations for both the rubidium and the ammonium salts are listed in Table 4. The atoms are labeled with numbers which identify their location in the unit cell, a portion of which is shown in Figure 2. The packing of $SbBr_6$ octahedra and rubidium ions can be seen in the stereo pair of Figure 3. The complete variance-covariance matrix was used in conjunction with ORFFE[17] in calculating the estimated standard deviations. The antimony-bromine bonding distances were corrected for thermal motion using the "riding model" approximation; no other distances were corrected for thermal motion.

The final parameters show that, within experimental error, both the $Sb^VBr_6{}^-$ and the $Sb^{III}Br_6{}^{3-}$ ions are distorted and possess D_{2d} symmetry. The mean length of the Sb^V--Br bond is 2.553 ± 0.005 Å perpendicular to the c-axis and is 2.640 ± 0.008 Å along the c-axis. The Br_1-Sb^V-Br_3 bond angle is

Table 4. Interatomic distances and angles and their estimated standard deviations

	Rubidium[a]	Ammonium[b]
Distance and angles within each anion:		
a) $Sb^{V}Br_6^{-}$		
$Sb - Br_1$	2.554 ± 0.005 Å	2.566 ± 0.006 Å
$Sb - Br_3$	2.640 ± 0.008	2.559 ± 0.005
$Br_1 - Br_3$	3.585 ± 0.006	3.739 ± 0.008
$Br_1 - Br_5$	3.565 ± 0.007	3.637 ± 0.009
$Br_1 - Sb - Br_3$	88.72 ± 0.13°	86.33 ± 0.15°
$Br_1 - Sb - Br_5$	90.029 ± 0.005°	90.23 ± 0.02°
b) $Sb^{III}Br_6^{3-}$		
$Sb - Br_2$	2.787 ± 0.004 Å	2.795 ± 0.006 Å
$Sb - Br_4$	2.713 ± 0.004	2.794 ± 0.005
$Br_2 - Br_4$	3.843 ± 0.004	3.963 ± 0.007
$Br_2 - Br_6$	3.934 ± 0.005	3.953 ± 0.009
$Br_2 - Sb - Br_4$	88.80 ± 0.06°	89.68 ± 0.13°
$Br_2 - Sb - Br_6$	90.025 ± 0.005°	90.002 ± 0.002°

---

[a] Riding model correction for thermal motion for Sb - Br bonds only.

[b] Rigid body libration correction for thermal motion in ammonium salt for all distances.

Table 4 (Continued)

	Rubidium[a]	Ammonium[b]
Environment of cation		
Rb - Br$_1$	3.797 ± 0.004 Å	3.96 ± 0.01 Å
- Br$_3$	3.997 ± 0.004	3.96 ± 0.02
- Br$_5$	4.060 ± 0.005	4.05 ± 0.02
- Br$_2$	3.790 ± 0.003	3.83 ± 0.01
- Br$_4$	3.658 ± 0.005 Å	3.58 ± 0.02 Å
- Br$_6$	3.586 ± 0.003	3.55 ± 0.02
- Br$_7$	3.797 ± 0.005	3.96 ± 0.01
- Br$_8$	4.06 ± 0.005	4.05 ± 0.02
- Br$_9$	3.997 ± 0.004	3.96 ± 0.02
- Br$_{10}$	3.586 ± 0.003	3.55 ± 0.02
- Br$_{11}$	3.658 ± 0.005	3.58 ± 0.02
- Br$_{12}$	3.790 ± 0.003	3.83 ± 0.01
Bromine-bromine contacts between anions (≤ 4.0 Å)		
Br$_2$ - Br$_3$	3.773 ± 0.007 Å	3.818 ± 0.008 Å
Br$_2$ - Br$_8$	3.829 ± 0.004	3.817 ± 0.008
Br$_6$ - Br$_{10}$	3.781 ± 0.004	3.649 ± 0.007
Br$_4$ - Br$_{11}$	3.781 ± 0.004	3.649 ± 0.007
Br$_3$ - Br$_8$	3.829 ± 0.004	3.881 ± 0.008
Bromine-bromine non-bonding distances between anions along the axes		
Br$_2$ - Br$_{15}$	5.145 ± 0.007 Å	5.13 ± 0.01 Å
Br$_4$ - Br$_{16}$	5.508 ± 0.009	5.479 ± 0.008
Br$_{13}$ - Br$_{14}$	5.667 ± 0.010	5.62 ± 0.01

Figure 3. A stereo pair of a portion of the unit cell showing the spacial arrangement of the rubidium cations to the antimony halide anions. The b-axis is across the page; the a-axis is vertical; and the c-axis is into the page. The bond distances are uncorrected for thermal motion. The unlabeled distances along the c-axis are 2.61 (Sb^{V}-Br) and 2.71 Å (Sb^{III}-Br)

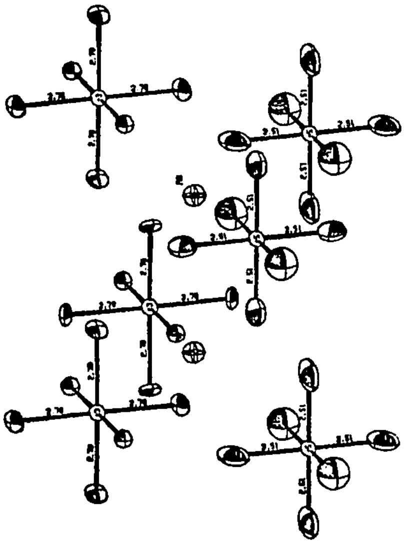

RB-4 SB(+3) SB(+5) BR-12

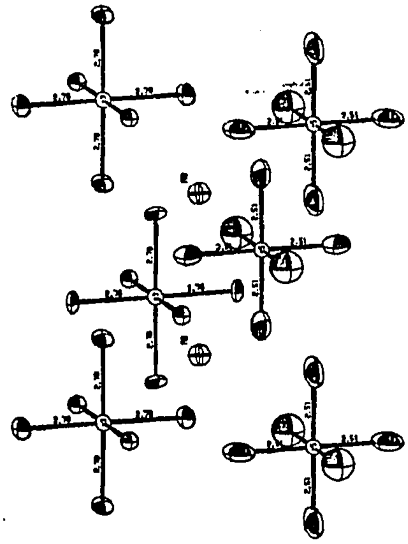

RB-4 SB(+3) SB(+5) BR-12

88.72 ± 0.13°. In the ammonium salt all the antimony(V) bromine distances were nearly equivalent and equal to 2.564 ± 0.006 Å. The same bond angle was 86.33 ± 0.15. Thus the distortions from O_h symmetry of the $Sb^{V}Br_6^-$ ion are quite different in the two salts.

The mean length of the Sb^{III}-Br bond is 2.787 ± 0.004 perpendicular to the c-axis and 2.713 ± 0.004 along the c-axis. The bond angle Br_2-Sb^{III}-Br_4 is 88.80 ± 0.06°. In the ammonium salt the $Sb^{III}Br_6^{3-}$ ion had O_h symmetry with bond distances of 2.795 ± 0.006 Å. The rubidium ion occupies a tetrahedral hole formed by four antimony halide groups, two $Sb^{V}Br_6^-$ and two $Sb^{III}Br_6^{3-}$. Three bromine atoms from each of the four groups form the 12 nearest neighbors.

The rubidium ion is fixed by symmetry along the c-axis, but has some freedom to move in the a-b plane. The closest distance between any one bromine atom in a $Sb^{V}Br_6^-$ ion and the rubidium ion is 3.797 Å and the closest distance of the same type with the $Sb^{III}Br_6^{3-}$ ion is 3.586 Å. The four shortest bromine-bromine distances between different $SbBr_6$ groups are 3.773 (Br_2-Br_3), 3.829 (Br_2-Br_8), 3.781 (Br_6-Br_{10} and Br_4-Br_{11}) and 3.829 Å (Br_3-Br_8). The first two distances are $Sb^{III}Br_6^{3-}$--$Sb^{V}Br_6^-$ closest contacts. The third and fourth correspond to the shortest bromine-bromine distances between different $Sb^{III}Br_6^{3-}$ anions and $Sb^{V}Br_6^-$ anions, respectively.

Within the $Sb^{V}Br_6^-$ ion the mean distance between bromines is 3.61 Å and within the $Sb^{III}Br_6^{3-}$ ion this distance is 3.90 Å. Since the contacts are much closer within the $Sb^{V}Br_6^-$ ion than in the $Sb^{III}Sb_6^{3-}$ ion, the motions of the individual bromine atoms in the former are probably coupled to a greater degree than in the latter. This coupling will cause librations of the anion and will affect the calculated antimony-bromine bond distances. The difference between the "riding model" correction (as used in this paper) and the "rigid body libration" correction is expected to be small and should not affect the over-all symmetry of each anion.

Discussion

The different volumes of the unit cells of $Rb_4Sb_2Br_{12}$ (2,486 $Å^3$) and $(NH_4)_4Sb_2Br_{12}$ (2,445 $Å^3$) can be understood assuming that in the ammonium ion the positive charge is partially localized on each of the hydrogen atoms. These localized positive charges, in a fixed orientation, can interact by Coulomb attraction with the anions causing a small contraction of the unit cell. This ordering occurs in NH_4Br.[19] In the spherically symmetric rubidium ion localization is not possible.

Although only small changes in unit cell dimensions are observed, large changes are found in the stereochemistry of both the $Sb^{V}Br_6^-$ and $Sb^{III}Br_6^{3-}$ ions. Neither van der Waal forces nor charge transfer effects through the rubidium ion are possible explanations of the observed distortions. The sum of ionic radii[20] of rubidium and bromide ions, 3.43 Å, is considerably shorter than any observed Rb-Br distance.

Electrostatic effects are a possible explanation for the distortions of the $Sb^{III}Br_6^{3-}$ ion. Table 4 shows that the average rubidium-bromine distance (3.815 Å) is nearly the same as in the ammonium salt (3.822 Å). Table 4 also shows that the intermolecular bromine-bromine distances between $Sb^{III}Br_6^{3-}$ anions has increased from 3.649 Å in the ammonium salt to 3.781 Å (Br_6-Br_{10}) in the rubidium salt, while all other bromine-bromine distances have remained almost constant. The shortening of the Sb^{III}-Br bond along the c-axis reduces the electrostatic repulsion while not affecting the attractions. The net result is a stabilization of the lattice.

The distortion of the $Sb^{III}Br_6^{3-}$ ion is, therefore, cation and packing dependent. The same result was found in the structure determination of $(C_5H_5NH)_6Sb^{III}Sb_3^{V}Br_{24}$.[3] The distortion could not be ascribed to the effect of the lone electron pair and thus to any seven-coordinated type of structure. The increase in Sb-Br distance going from Sb^{V} to the Sb^{III} ion (about 0.2 Å), which is greater than that expected due to the charge difference, suggests the lone pair exists in a spherically symmetric state. This conclusion agrees with the work of Day[2] and with the suggestion of Urch,[21] that a lone electron pair can be accommodated in the a_{1g} antibonding orbital and not cause distortions from O_h symmetry.

The distortion of the $Sb^VBr_6^-$ ion might be indicative of charge transfer paths linking the pentavalent antimony bromines along the c-axis to the trivalent antimony anions. However, it might also be simply indicative of bromine-bromine repulsions in this ion. These distances are 3.771 Å (Br_2-Br_3) and 3.829 Å (Br_2-Br_8). The strength of the former argument is rather weak since these two distances are only 0.13 and 0.07 Å shorter than the sum of two bromide ionic radii (3.90 Å); they are also quite similar to the shortest bromine-bromine distances between like anions. Yet the expansion of the Sb^V-Br bond along the c-axis suggests that there is some interaction between the $Sb^VBr_6^-$ ion and its neighbors. No other explanation is apparent to explain the black color, other than the charge transfer which may occur by the paths described above.

MOLECULAR BROMINE BRIDGING OF $Sb_2^{III}Br_9^{3-}$ ANIONS AND THE CRYSTAL STRUCTURE OF $[(CH_3)_4N]_3Sb_2Br_{11}$

Introduction

The crystal structure of tetramethylammonium nonabromodiantimonate(III) dibromine, $[(CH_3)_4N]_3Sb_2Br_{11}$, was undertaken as part of a series of structure investigations of halo-coordinated antimony compounds.[1,3-5,22-27] Numerous intensely colored compounds of the type $R_xSb_yBr_z$, where R is an aliphatic amine, aromatic amine, alkali metal, or ammonium cation, have been widely studied since 1901 when Rosenheim and Stellman[28] reported the preparation of $(C_5H_5NH)_2SbBr_7$. The wide variety of related compounds[29] include: $RSbBr_4$; $RSbBr_6$; $RSbBr_7$; R_2SbBr_5; R_2SbBr_6; R_2SbBr_7; R_2SbBr_8; R_2SbBr_9; R_3SbBr_6; $R_2Sb_2Br_7$; $R_3Sb_2Br_{11}$; $R_3Sb_2Br_{12}$; $R_3Sb_2Br_{15}$; $R_2Sb_3Br_{11}$; $R_5Sb_3Br_{14}$; $R_7Sb_3Br_{16}$ and $R\cdot SbBr_3\cdot 3HBr$. The intense dark color common to many $R_xSb_yBr_z$ compounds has been attributed[30] to charge transfer between mixed oxidation states of antimony or to some other charge transfer phenomena.

In this laboratory a series of structural investigations of antimony halide complexes have been performed to elucidate, if possible, the charge transfer path and to investigate the wide variety of complexes attainable in the solid state by merely varying the cation used. In addition, the structural information may lead to a general description of antimony halide bonding.

The structure determination of a red tetramethylammonium salt was undertaken as a result of preliminary investigations of several intensely colored $R_xSb_yBr_z$ complexes. Two $(CH_3)_4N^+$ salts exist: a black salt which decomposed when exposed to X-rays and a very stable[5] red salt. The stoichiometry of the red form was reported[31] to be $R_3Sb_2Br_{11}$.

Experimental

Crystal data:

Tetramethylammonium nonabromodiantimonate(III) dibromine, $[(CH_3)_4N]_3Sb_2Br_9\cdot Br_2$, Mw = 1345, Hexagonal $P6_3/mmc$, Z = 2, $\underline{a} = \underline{b} = 9.5850 \pm 0.0005$ Å, $c = 22.6667 \pm 0.0026$ Å, $T \approx 24°C$, Dm = 2.55 g/cc, Dc = 2.48 g/cc, MoK_α (λ = 0.7107 Å), μ = 148.6 cm^{-1}.

The clear red $[(CH_3)_4N]_3Sb_2Br_{11}$ crystals were prepared by the method of Hackert et al.[5] Microscopic examination revealed the six fold symmetry of the crystals which grew as hexagonal plates with sharply defined faces. As the crystals were found to be air stable they were mounted on glass fibers. The preliminary Weissenberg and precession photographs exhibited 6/mmm Laue symmetry. The following systematic absence was observed: $\underline{hh2\bar{h}\ell}$ when $\underline{\ell} = 2n + 1$. The Laue symmetry and systematic absence are consistent with the following space groups: $P6_3/mmc$ $P\bar{6}2c$, or $P6_3mc$. The diffraction pattern was quite weak and numerous reflections were accidentally absent. Four day precession photographs did not reveal any previously unobserved systematically weak reflections relating to a pseudo cell as was found in $Rb_4Sb^{III}Sb_VBr_{12}$.

The unit cell parameters and their standard deviations were obtained by a least squares fit[8] to thirteen independent reflections angles whose $+2\theta$ and -2θ centers were determined by a left-right, top-bottom beam splitter technique using a previously aligned Hilger-Watts automated four circle diffractometer (MoK_α radiation, $\lambda = 0.71069$ Å). The calculated density of 2.48 g/cc for 2 molecules per unit cell agrees well with the observed density of 2.55 ± 0.1 g/cc which was determined by flotation techniques. To obtain adequate counting statistics, a crystal having approximate dimensions 0.19 x 0.16 x 0.11 mm along the a, b and c axes, respectively, was used for data collection. Data were collected at room temperature utilizing the Hilger-Watts diffractometer equipped with scintillation counter and employing Zr-filtered MoK_α radiation. All data within the $hk\ell$ 'octant' were recorded within a two-theta sphere of 50°. As nearly all intensities from 40 to 50° 2θ were found to be at background level, data from the equivalent 'octants' $\bar{h}\bar{k}\bar{\ell}$ and $h\bar{k}\ell$ was recorded within the two-theta sphere of 40°. A total of 2748 reflections were recorded using the θ-2θ scan technique with a take-off angle of 4.5°.

Symmetric scans ranged from 1.0° in 2θ at low two theta to 2.0° at large two theta. The stepping rate was 0.4096 sec/step of 0.02° in two theta. Stationary-crystal, stationary-counter background counts were measured at each end of the scan for half the time of the scan. Three standard reflections were observed periodically, and these observations indicated that no decomposition occurred during data collection.

The intensity data were corrected for Lorentz-polarization effects and for absorption ($\mu = 148.6\ \mathrm{cm}^{-1}$). The absorption correction[32] was calculated using ABCOR;[12] the maximum and minimum transmission factors were 0.227 and 0.123, respectively. The estimated error in each intensity was calculated by

$$\sigma_I^{\,2} = [C_T + C_B + (0.03C_T)^2 + (0.05C_B)^2 + (0.10C_I)^2]/A$$

where C_T, C_B, C_I and A are the total count, background count, net count and transmission factor, respectively. The quantities 0.03, 0.05 and 0.10 represent estimates for non-statistical errors in the total count, background count and absorption correction, respectively. The estimated standard deviation σ_F for each structure factor was calculated using the method of finite differences.[11]

No significant differences could be found between Friedel related pairs of observed structure factors; the lack of apparent anomalous dispersion effects indicates that the space group is probably centric. The equivalent data were then averaged. The estimated standard deviation $\bar{\sigma}_F$ in each averaged structure factor was taken as the root mean square of the individual σ_F's. Of the total 720 independent reflections ($h \geqq k \geqq 0$) only 286 reflections were considered observed ($\geqq 3\bar{\sigma}_F$). The overall internal agreement, $R_F = 0.086$,[†] was not unexpectedly high since there was a large fraction of unobserved reflections. The 286 observed data were used in the least-squares refinement with the reciprocals of $\bar{\sigma}_F^{\,2}$ used as weights.

Solution and Refinement

A Patterson map was computed by a Fourier program written by the author specifically for the hexagonal symmetry. Analysis of the heavy atom vectors in this map indicated the presence of a center of symmetry, and hence the space group was assumed to be $P6_3/mmc$. An equivalent result was also obtained by a statistical test[33] and was confirmed by successful refinement in this space group. (Attempted refinement in space groups $P6_3mc$ and $P\bar{6}2c$ revealed unusual coupling of thermal and positional parameters.) The Patterson map clearly revealed the Sb_2Br_9 moiety. The two remaining bromine atoms

---

[†] $$R_F = \sum_{i=1}^{720} \sum_{j=1}^{NE_i} \left[(|F_{ij} - \bar{F}_i|)^2 / \bar{\sigma}_{F_i}^{\,2} \right] \Big/ \left[\sum_i NE_i \, \bar{F}_i^{\,2} / \bar{\sigma}_{F_i}^{\,2} \right] ,$$

where NE_i is the number of equivalent data for independent reflection i.

could not be located; however, there was a set of six unique peaks with peak heights corresponding to $\frac{1}{3}$ (Br-Br) vectors. A structure factor difference electron density map calculation clearly indicated the presence of a three fold disordered bromine molecule. All heavy atom positions and isotropic temperature factors were then refined by full-matrix least-squares techniques to a conventional discrepancy factor of $R = \Sigma||F_o|-|F_c||/\Sigma|F_o| = 0.197$ and a weighted R-factor of $wR = \{\Sigma w(|F_o|-|F_c|)^2/\Sigma wF_o{}^2\}^{1/2} = 0.213$. A difference electron density map indicated appreciable anisotropic thermal motion and diffuse peaks attributable to disordered tetramethylammonium cations. Anisotropic refinement of the heavy atoms lowered R to 0.167 and wR to 0.186. Throughout the refinement the scattering factors for Sb^{3+}, Br^-, C and N reported by Cromer and Waber[34] were used. Both Sb and Br were modified for the real and imaginary parts of anomalous dispersion.[15] The disordered cations were located by repeated difference map calculations.

The two symmetry independent cations exhibit site disorder as well as considerable thermal motion. Although the cation models given in Table 5 were determined through difference map calculations, they could not be satisfactorily refined by least squares techniques. The models were constrained to closely represent NC_4 tetrahedra with C-N distances ≈ 1.54 Å. The thermal parameters were selected to best fit the

Table 5. Cation parameters

Cation	Atom[a]	Occupancy	x[b]	y	z	B
1[c]	N	1/4	0.0	0.0	0.237	6.0
	Cl	1/4	0.0	0.0	0.170	10.0
	C3	1/4	0.172	0.156	0.25	5.0
2[c]	N	1/4	0.0	0.0	0.258	5.0
	Cl	1/4	0.0	0.0	0.190	10.0
	C3	1/4	0.088	0.176	0.281	7.0
3-4	N	1	1/3	2/3	-0.086	10.0
	Cl	1	1/3	2/3	-0.154	10.0
	C3	1/2	0.25	0.50	-0.059	7.0
	C3	1/2	0.424	0.848	-0.063	7.0

[a] N and Cl lie on the 6_3 axis (cation 1 and 2) or the $\bar{6}$ axis (cations 3 and 4). The remaining three carbons of the cation are related to C3.

[b] x,y,z are fractional unit cell coordinates.

[c] Cations 1 and 2 exhibit further disorder due to the mirrors at z = 1/4 and 3/4.

electron density map. Including the cations lowered R to 0.137 and wR to 0.125.

The final difference map revealed no peaks higher than 1.8 e/Å^3. However, diffuse peaks of $\sim$ 1 e/Å^3 could be seen in proximity to the cations indicating that the cation model only approximately represented the true disorder. The author feels that further efforts to represent the cation disorder is not warranted. In the last cycle of refinement the largest shift in any parameter was less than 0.01 times its own e.s.d. The final heavy atom parameters are given in Table 6, along with their estimated standard deviations as derived from the inverse matrix. Table 7 lists the magnitudes of the observed and calculated structure factors. The computer drawings shown throughout the following text were made using ORTEP.[18] Distances, angles, and their standard deviations were calculated by ORFFE[17] using the variance-covariance matrix from the final least-squares cycle.

Description of the Structure

The unit cell contains two $Sb_2^{III}Br_9^{3-}$ anions, two bromine molecules and six cations. The anions throughout the crystal are bridged by Br_2 molecules, forming an infinite 3-dimensional network. The important bond distances and angles are summarized in Table 8. The molecular bromines are labeled Br^m and the bridging and terminal anion bromines are labeled Br^b and Br^t, respectively. The stereo pair (Figure 4) shows one Br_2 bridge between anions. Each Br^t is a possible bridging site. However, due to the disorder of the Br^m atoms and steric effects each anion is bridged to only two other anions.

Table 6. Heavy atom positional[a] and thermal[b] parameters and their standard errors[c] for $[(CH_3)_4N]_3Sb_2Br_{11}$

Atom	Site	x	y	z	β_{11}	β_{22}	β_{33}	β_{12}	β_{13}	β_{23}
Br^m	12k	0.0573(9)	2x	0.0287(7)	0.030(3)	0.021(3)	0.0042(6)	$\frac{1}{2}\beta_{22}$	$\frac{1}{2}\beta_{23}$	-0.001(1)
Br^t	12k	0.0202(4)	2x	0.0996(3)	0.033(1)	0.027(2)	0.0066(3)	$\frac{1}{2}\beta_{22}$	$\frac{1}{2}\beta_{23}$	-0.0033(5)
Br^b	6h	0.4741(5)	2x	1/4	0.031(2)	0.021(2)	0.0057(3)	$\frac{1}{2}\beta_{22}$	0	0
Sb	4f	1/3	2/3	0.1641(3)	0.0205(9)	β_{11}	0.0049(2)	$\frac{1}{2}\beta_{11}$	0	0

[a] Positional parameters are in fractional unit cell coordinates.

[b] β's x 10^4; The form of the anisotropic temperature factor is $\exp[-(\beta_{11}h^2 + \beta_{22}k^2 + \beta_{33}\ell^2 + 2\beta_{12}hk + 2\beta_{13}h\ell + 2\beta_{23}k\ell)]$.

[c] Estimated standard deviations are given in parentheses for the least significant figures.

Table 7. Observed and calculated structure factors in electrons

L = 0

H	K	FO	FC
1	0	102	62
2	0	24	5
3	0	13	19
4	0	22	23
5	0	16	26
6	0	44	46
7	0	57	55
8	0	27	30
1	1	249	202
2	1	78	65
3	1	148	133
4	1	78	81
5	1	54	57
6	1	52	46
7	1	63	72
2	2	334	331
3	2	182	193
4	2	45	46
5	2	19	10
3	3	148	159
5	3	23	26
6	3	40	39
4	4	37	30
5	5	69	62

L = 1

H	K	FO	FC
1	0	248	247
2	0	34	41
3	0	31	20
4	0	43	47
5	0	18	11
7	0	82	82
8	0	28	40
2	1	36	35
3	1	121	97
6	1	43	49
3	2	206	203
4	2	58	58
5	2	23	15
6	2	32	33
8	2	29	1
4	3	17	4
5	4	41	45

L = 2

H	K	FO	FC
0	0	70	59
1	0	126	152
2	0	140	116
3	0	54	47
4	0	53	54
5	0	63	69
6	0	61	68
1	1	15	9
2	1	153	143
4	1	57	61
5	1	26	23
6	1	18	9
7	1	24	26
8	1	31	3
2	2	130	126
3	2	20	6
4	2	32	22
5	2	31	30
3	3	48	48
4	3	19	17
4	4	33	29
5	4	24	18

L = 3

H	K	FO	FC
1	0	55	83
2	0	235	222
3	0	227	240
4	0	33	34
5	0	40	44
6	0	37	46
2	1	54	45
3	1	36	34
4	1	133	119
6	1	39	37
7	1	27	7
8	1	27	5
3	2	46	41
5	2	64	67
6	2	23	18
7	2	32	14
4	3	26	25
5	3	40	41

L = 4

H	K	FO	FC
0	0	131	99
1	0	117	122
2	0	333	336
3	0	45	49
4	0	106	92
5	0	108	106
6	0	30	22
1	1	35	31
2	1	87	83
3	1	53	53
4	1	79	78
5	1	17	25
6	1	36	30
7	1	21	26
2	2	75	84
3	2	46	45
4	2	40	39
5	2	35	32
3	3	80	86
5	3	39	43
6	5	37	10

L = 5

H	K	FO	FC
1	0	93	88
2	0	107	110
3	0	75	77
4	0	51	38
5	0	133	132
6	0	21	23
2	1	145	139
3	1	83	86
4	1	17	16
5	1	47	45
6	1	39	35
4	2	56	56
5	2	54	51
6	2	27	23
7	2	43	33
4	3	64	66
5	3	39	38
6	4	32	15
7	4	33	4
6	5	31	12

L = 6

H	K	FO	FC
0	0	251	243
1	0	37	36
2	0	74	79
3	0	216	222
4	0	102	103
5	0	93	99
6	0	43	52
1	1	215	224
2	1	122	114
4	1	63	71
5	1	32	40
6	1	24	23
2	2	25	22
3	2	26	23
4	2	50	54
5	2	69	74
6	2	30	34
4	3	43	42
5	3	26	19
4	4	53	53

L = 7

H	K	FO	FC
1	0	49	43
2	0	209	222
3	0	77	80
4	0	127	131
5	0	59	63
2	1	126	124
3	1	30	31
5	1	104	105
8	1	74	20
3	2	49	56
4	2	24	20
6	2	22	25
4	3	73	69
5	3	39	40

L = 8

H	K	FO	FC
0	0	153	145
2	0	99	97
3	0	75	82
4	0	58	38
1	1	34	89
2	1	15	17
3	1	18	3
4	1	26	36
5	1	24	23
2	2	54	51
3	2	23	24
4	2	25	23
5	2	26	36
8	2	30	11
4	3	21	17
4	4	30	16

L = 9

H	K	FO	FC
1	0	16	10
2	0	72	76
3	0	122	127
4	0	47	42
5	0	51	56
7	0	26	25
8	0	34	7
3	1	17	18
4	1	28	25
5	1	44	37
3	2	20	19
5	2	44	46
6	2	21	5

L = 10

H	K	FO	FC
1	0	34	30
2	0	112	115
3	0	70	74
4	0	27	21
5	0	84	91
6	0	34	38
1	1	75	85
2	1	106	110
4	1	21	27
7	1	28	8
2	2	38	38
5	2	30	26
6	2	33	23
7	2	31	14
4	3	33	38
7	3	31	9

L = 11

H	K	FO	FC
1	0	48	39
2	0	114	115
3	0	54	55
4	0	42	42
5	0	26	27
6	0	20	17
2	1	17	21
3	1	58	61
4	1	55	57
6	1	43	40
3	2	35	35
4	2	45	46
6	2	32	7
5	3	33	28

L = 12

H	K	FO	FC
0	0	163	168
1	0	91	92
2	0	16	8
3	0	28	30
4	0	22	13
6	0	31	32
1	1	43	43
2	1	24	25
3	1	39	38
4	1	50	53
6	1	20	3
7	1	29	27
2	2	30	92
3	2	40	37
5	2	21	21
3	3	59	55
4	3	20	15

L = 13

H	K	FO	FC
1	0	94	95
2	0	32	21
4	0	19	19
6	0	25	17
7	0	30	35
2	1	17	11
3	1	24	24
4	1	22	14
5	1	20	5
3	2	91	70
4	3	28	5

L = 14

H	K	FO	FC
0	0	163	159
2	0	24	28
4	0	20	2
5	0	21	8
6	0	19	5
2	1	27	19
3	1	23	15
2	2	62	57
3	2	35	33
3	3	23	11
5	3	27	2

L = 15

H	K	FO	FC
3	0	20	17
4	0	26	16
2	1	18	16
3	2	24	8
6	3	38	1

L = 16

H	K	FO	FC
0	0	78	65
2	0	49	40
4	0	33	27
6	0	29	2
1	1	40	46
2	1	32	19
3	1	26	21
6	1	28	11
3	2	25	20
3	3	26	18

L = 17

H	K	FO	FC
1	0	34	36
2	0	39	29
5	0	29	24
6	0	28	2
2	1	30	30
3	1	26	17
4	1	22	16
5	2	29	14

L = 18

H	K	FO	FC
1	0	20	25
2	0	48	42
3	0	28	22
4	0	25	16

L = 19

H	K	FO	FC
4	0	29	10
2	1	20	13
3	1	23	10

L = 20

H	K	FO	FC
2	0	21	1
4	0	30	8
6	0	38	1
5	1	31	4

L = 22

H	K	FO	FC
-3	2	36	5

Table 8. Selected bond distances and angles

Atoms[a]	Bond distance[b]	Atoms[a]	Bond angle[b]
Br^{m}-Br^{m*}	2.31(3) Å	Br^{m*}-Br^{m}...Br^{t}	179.4(6)°
Br^{m}...Br^{t}	2.89(1)	Br^{m}...Br^{t}-Sb	179.9(5)
Br^{t}-Sb	2.625(8)	Br^{t}-Sb-Br^{b}	174.0(3)
Br^{t}...$Br^{t\dagger}$	3.77(1)	Sb-Br^{b}-$Sb^{\ddagger}$	79.6(3)
Sb-Br^{b}	3.043(8)	Br^{b}-Sb-$Br^{t\dagger}$	93.1(2)
Sb...$Sb^{\ddagger}$	3.89(2)	$Br^{t\dagger}$-Sb-Br^{t}	92.0(3)
		$Br^{b\dagger}$-Sb-Br^{b}	83.4(2)

[a] Symmetry operations:

$^{*}(xyz)\rightarrow(\bar{x}\bar{y}\bar{z})$

$^{\dagger}(xyz)\rightarrow(1-y,\ 1-x,z)$

$^{\ddagger}(xyz)\rightarrow(x,y,\frac{1}{2}-z)$

[b] Estimated standard deviations are given in parentheses for the least significant figures.

The presence of molecular bromine was reported in $(C_7H_{13}NH)_4Sb^{III}Sb^{V}Br_{12}\cdot 2Br_2$.[27] However, the role of the Br_2 molecule was unclear due to disorder of both Sb octahedra and the Br_2 species. In the tetramethylammonium salt the molecular bromine bond distance is 2.31(3) Å. This distance is quite

Figure 4. Stereo pair of a Br_2 bridge between $Sb_2Br_9^{3-}$ anions

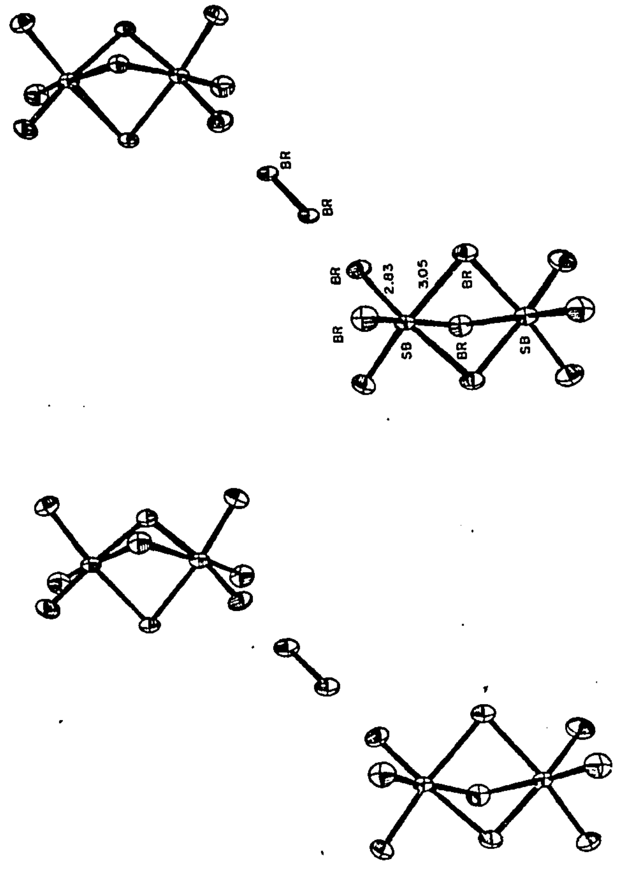
BR
BR
BR
2.83
3.05
BR
BR
SB
BR
SB

dependent on the cation model - it ranged from 2.34 to 2.28 Å while testing cation models. The Sb_2Br_9 atom positions were quite insensitive to the cation model. The Br-Br distance in $(C_7H_{13}NH)_4Sb^{III}Sb^{V}Br_{12}\cdot 2Br_2$ was 2.32(4) Å, possibly lengthened over the crystalline bromine distance of 2.27 Å.[35]

The $Sb_2Br_9{}^{3-}$ anion has D_{3h} symmetry. The bond distances and angles are quite similar to those observed in $(C_5H_5NH)_5Sb_2Br_9\cdot(Br)_2$.[23] There is a slight lengthening of the $Sb-Br^b$ distance (3.04 vs 3.00 Å), a decrease in the Sb...Sb distance (3.89 vs 4.01 Å) and a corresponding decrease in the $Sb-Br^b-Sb$ angle (79.6 vs 83.7°). The $Sb-Br^t$ distance appears unchanged (2.63 Å). The Br-Sb-Br...Br-Br... chain is nearly linear: $\sphericalangle(Br^b-Sb-Br^t)$ = 174.0(3)°; $\sphericalangle(Sb-Br^t...Br^m)$ = 179.9(5)°; and $\sphericalangle(Br^t...Br^m-Br^m)$ = 179.4(6)°. The Br_2 molecule bridges two anions, and lies perpendicular to four other $Sb-Br^t$ bonds. The $Br^t...Br_2$ distance along the bridged chain is only 2.89(1) Å.

The cations fill large holes between the anions. The closest C...Br contact is 3.3 Å. However, most C...Br contacts are $\geq$ 3.95 Å, the sum of CH_3 and Br van der Waal radii.[36] Two projections of the unit cell contents are given in Figures 5a and 5b. A half cell ($0 \leq z \leq \frac{1}{2}$) projection onto the a-b plane is given in Figure 5a. The projection down the b* axis onto the a-c plane is shown in Figure 5b. In these figures the large open circles (radius = 1.5 Å) are the cations located on

Figure 5. Unit cell projections of $[(CH_3)_4N]_3Sb_2Br_{11}$

a) A half cell ($0 \leq z \leq \frac{1}{2}$) projection onto the a-b plane

b) Projection down the b* axis onto the a-c plane

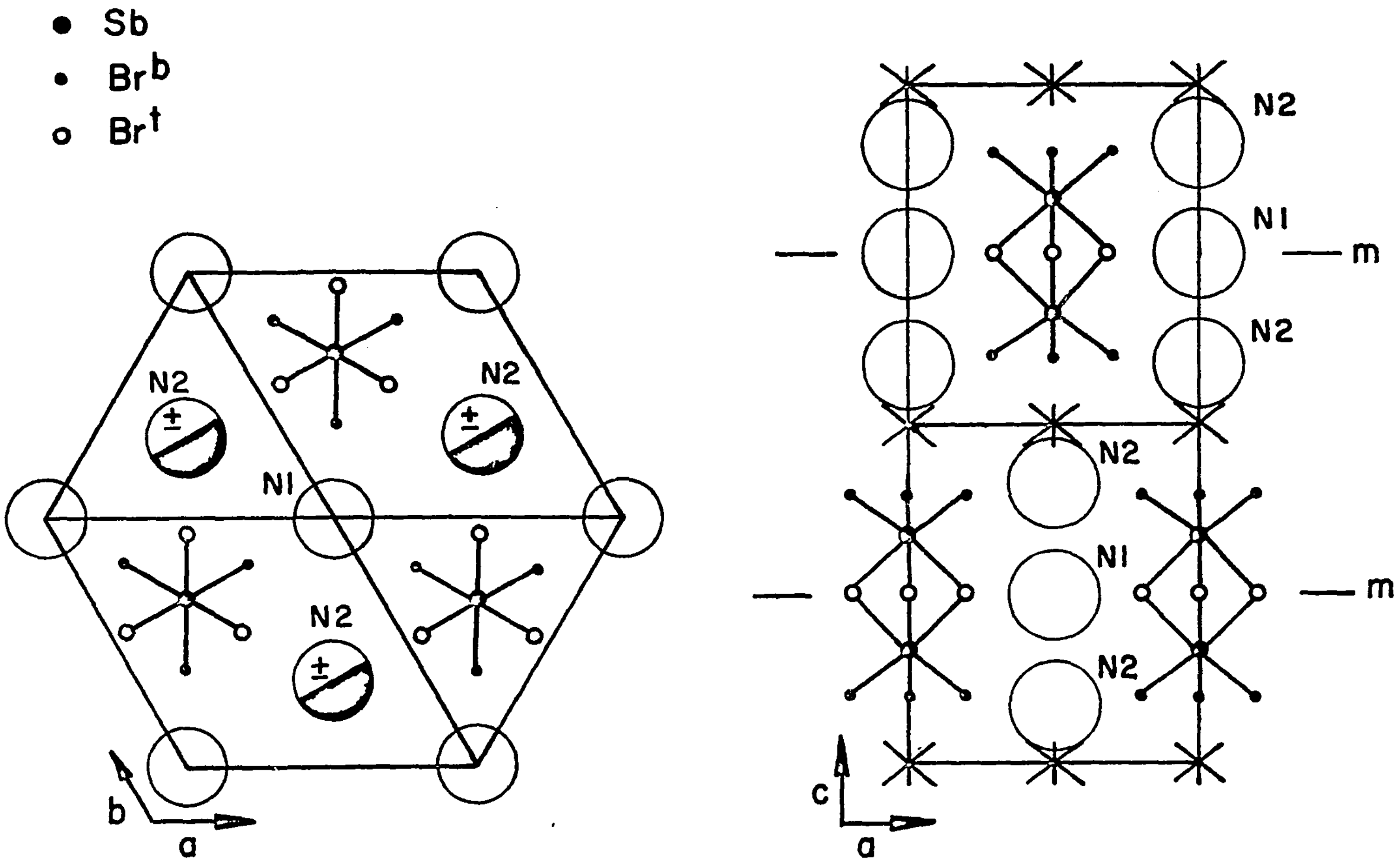
● Sb
• Br^b
○ Br^t
N2
N2
N1
N2
±
b
a
N2
N1
N2
m
N2
N1
N2
m
c
a

the mirrors at $z = \frac{1}{4}$. The large half open circles are the remaining cations. The small open circles are the bridging anion bromines. The small black circles are the terminal anion bromines. The disordered bromine molecules are omitted in Figure 5a for clarity. The observed disorder and large thermal motion of the cations is probably the result of the lack of directional binding and the large available volume between anions.

Discussion

The shortness of the $Br^{t}...Br^{m}$ distance, approximately 1 Å shorter than the sum of bromine van der Waal radii,[36] is indicative of an important interaction between the bromine molecule and the Sb_2Br_9 anions. This distance is 0.13 Å shorter than the 3.02 Å of the proposed $Sb^{III}Br...Br_2$ interaction in $(C_7H_{13}NH)_4Sb^{III}Sb^{V}Br_{12}\cdot 2Br_2$.[27] The shortest reported Br...Br contact (other than in these two Br_2 bridged compounds) is 3.14 Å in PBr_7.[37]

The Br_2 bridge produces a chain of at least twelve atoms. This chain consists of three linear fragments; the eight atom central fragment includes the molecular bromine. The site disorder of Br_2 prevents us from definitely defining the chain length - some chains may of course be of much longer length. The possibility of a super cell (a' = 3a) containing ordered Br_2 molecules cannot be definitely eliminated. However, no evidence was found for its existence.

A black tetramethylammonium salt is known to exist which readily debrominates to form a red solid.[5] This leads one to speculate that the black salt could contain $Sb_2Br_9{}^{3-}$ anion with all Br^t sites saturated with Br_2 bridges.

The bonding of the $Sb_2{}^{III}Br_9{}^{3-}$ anion and the molecular bromine bridge is of some interest. To a first approximation, the bonding in antimony(III) bromide salts can be explained completely through use of p orbitals and multicenter bonds. For example, it has been suggested[23] that the $Sb_2{}^{III}Br_9{}^{3-}$ moiety consists of six three-center four-electron bonds (Br^b-Sb-Br^t). The Sb^{III} lone pair of electrons was assigned to the spherical s orbital. In this structure, electron donation from the 'non-bonding' σ orbital of the three-center four-electron bond to the antibonding σ orbital of Br_2 is possible. Although lengthening of the Br_2 bond was observed for some cation models, the uncertainty in this distance prevents a definite conclusion from being drawn. The shifts in bond distances and angles of the $Sb_2Br_9{}^{3-}$ anion are probably due to crystal packing forces. The stability of the title compound can be in part due to the postulated Br_2 bridge. In addition, this bridging model predicts that $[(CH_3)_4N]_3Sb_2Br_{11}$ should be a semiconductor or a weak conductor.

A HIGHLY EFFICIENT NEUTRON DIFFRACTION TECHNIQUE - USE OF WHITE RADIATION

Introduction

A major limitation in single-crystal neutron diffraction studies is the relatively low flux of the neutron beams employed. To obtain adequate counting rates large single crystals are usually required. These crystals are often difficult to obtain and can exhibit appreciable secondary extinction effects. In particular, hydrogen-containing compounds must be deuterated to avoid the strong effective absorption resulting from hydrogen incoherent scattering.

The inefficient methods presently used contribute greatly to the low flux of the neutron beam. The conventional monochromatic beam technique is poor in this sense. Monochromatic crystals are never totally efficient diffractors and "see" only a very small effective source at the reactor core due to the small mosaic spread of the crystal. The time of flight (TOF) technique does not provide an improvement over monochromatic beams due to the necessarily low efficiency of Fermi choppers. Alternate methods using Fourier choppers[38] and correlation choppers[39] are being tested experimentally. These choppers are $\sim$ 25% efficient, and a large increase in incident flux can be expected. However, sophisticated electronics are required, and results to date are not impressive.

The Laue diffraction method can be used to greatly increase the incident flux, and, consequently, smaller crystals can be studied at faster data rates. The large increase in flux results from several factors. First, the inefficiency of a crystal monochromator (or chopper) is eliminated. Second, the effective source of the incident beam can be much larger than that "seen" by a monochromating crystal. Finally, the neutron path length from the reactor core to the sample crystal can be a minimum since secondary equipment (such as a monochromator or chopper) is eliminated. The diffracted intensity is also enhanced by two other effects. First, each integrated intensity can be measured with a single peak height measurement[40] due to a wavelength integration. Second, each Laue intensity consists of a summation of intensities from many structure factors with identical Miller indexes.

The application of the white radiation neutron spectrum was discussed by Lowde.[41] However, the analysis of the resulting intensities was considered a fundamental weakness of the method. Lowde did not resolve this problem and a monochromatic beam from a high flux reactor was considered necessary for neutron diffraction studies of most materials. In the white radiation method presented here each Laue intensity is measured at selected scattering angles. By coupling the theta and omega diffractometer axes, each Laue intensity may be considered a "Laue streak". The overlap of intensity from several wavelengths causes minimal difficulty in the data analysis. Structure factors obtainable from the observed intensities are used to determine the structural model. This model is subsequently refined by a least-squares analysis based on observed and calculated intensities. Included in the calculated intensities are wavelength-dependent corrections for extinction and absorption.

Theory

In this section is given the mathematical formulation of the intensity equation, extinction correction, absorption correction and incident flux equation pertinent to the use of a polychromatic neutron beam for crystal structure determination. Corrections for inelastic scattering and multiple Bragg scattering are assumed to be negligible. Techniques for obtaining and refining structural models are also discussed.

Intensity formula

Each Laue spot can be measured at various scattering angles θ using a polychromatic beam and the bisecting orientation. The observed intensity consists of a summation of intensities resulting from all structure factors with Miller indexes $\underline{h}' = (h'k'\ell')$ scattering at the same Bragg angle.

$$I_{\underline{h}'}^{obs}(\theta) = \sum_{\underline{n}} I_{\underline{nh}}(\theta) \tag{1}$$

where the crystallographic indexes $\underline{nh} = (nh', nk', n\ell')$. The individual intensity terms $I_{\underline{nh}}$ are derived below following the procedure of Buras et al.[42] for the TOF spinning crystal technique.

The integrated intensity for Bragg diffraction using a monochromatic beam-rotating crystal method is given by

$$i_{\underline{h}}(\theta) = k\Phi(\lambda)\lambda^3 F_{\underline{h}}^{\,2}\, T(\lambda)y(\lambda)/\sin 2\theta, \tag{2}$$

where k is a scale factor, $F_{\underline{h}}$ is the structure factor, $T(\lambda)$ is an absorption correction, $y(\lambda)$ is an extinction correction, θ is the Bragg angle and $\Phi(\lambda)$ is the flux at wavelength λ. The intensity terms $I_{\underline{nh}}(\theta)$ are obtained by integration of $i_{\underline{nh}}(\theta)$ over the wavelengths accepted by the counter.

$$I_{\underline{nh}}(\theta) = k \int_{\lambda_{min}}^{\lambda_{max}} \Phi(\lambda)\lambda^3 F_{\underline{nh}}^{\,2} T(\lambda)y(\lambda)\, \frac{d\lambda}{\sin 2\theta}\ , \tag{3}$$

where λ_{min} and λ_{max} are determined by Bragg's equation for the finite counter aperature 2δ centered about θ. When the variable $d\lambda$ is changed to $d\theta$ using $d\lambda = \lambda\cot(\theta)d\theta$ from Bragg's law and when one realizes that $\Phi(\lambda)$, $y(\lambda)$, $T(\lambda)$ and $\sin^2\theta$ are essentially constants over the small angular range involved,

$$I_{\underline{nh}}(\theta_o) = k\lambda_n^{\,4}\ \Phi(\lambda_n)F_{\underline{nh}}^{\,2}T(\lambda_n)y(\lambda_n)\delta/\sin^2\theta_o \tag{4}$$

where $\lambda_n = 2d_{\underline{nh}}\sin(\theta_o)$. By substituting Equation 4 into Equation 1, defining $\Phi_{eff}(\lambda) = \lambda^2\Phi(\lambda)$, and replacing

$\lambda^2/\sin^2(\theta_o)$ with $(2d_{\underline{\underline{nh}}})^2$, one obtains the final form of the intensity equation

$$I_{\underline{h}'}(\theta_o) = K \sum_n \Phi_{eff}(\lambda_n)T(\lambda_n)y(\lambda_n)(F_{\underline{\underline{nh}}}d_{\underline{\underline{nh}}})^2 \qquad (5)$$

Extinction

Since the extinction correction varies with wavelength, this correction can be important in the white radiation method. Assuming that primary extinction can be neglected, the secondary extinction correction can be calculated using the Zachariasen[43] approximation

$$y(\lambda) = \left\{1 + 2rQ_o\bar{\bar{T}}/[\lambda^2 + r^2/g^2]^{1/2}\right\}^{-1/2} \qquad (6)$$

In this expression $Q_o = \lambda^3 F_c{}^2/[V_c{}^2 \sin(2\theta)]$, r and g are defined as the domain radius and Gaussian distribution parameters respectively, and $\bar{\bar{T}}$ is the absorption weighted path length.

The white radiation data can be sufficient to simultaneously determine both r and g.[44] However, in practice often either $r \gg \lambda g$ or $\lambda g \gg r$. In either case the extinction correction is a function of only one parameter.

$$\begin{array}{ll} r \gg g\lambda & \\ \text{(Type I)} & y(\lambda) = \left\{1 + 2gQ_o\bar{\bar{T}}\right\}^{-1/2}, \\ \lambda g \gg r & \\ \text{(Type II)} & y(\lambda) = \left\{1 + 2rQ_o\bar{\bar{T}}/\lambda\right\}^{-1/2}. \end{array} \qquad (7)$$

Attenuation

Attenuation of the incident and diffracted beam within the crystal results from two effects - true absorption and incoherent scattering. The linear absorption coefficient for true absorption μ^{abs} varies linearly with wavelength for nearly all elements (exceptions are the highly absorbing elements such as Cd or Gd). This linear relation is

$$\frac{\mu^{abs}}{\mu_o^{abs}} = \lambda/\lambda_o, \tag{8}$$

where μ^{abs} and μ_o^{abs} correspond to wavelength λ and λ_o respectively.

Attenuation due to incoherent scattering is wavelength independent for nearly all elements. However hydrogen is an important exception. In the next section hydrogen incoherent scattering is shown to increase approximately linearly with wavelength. The cumulative effect of both true absorption and incoherent scattering expressed in terms of the linear attenuation coefficient is

$$\mu = \mu^{abs} + \mu^{incoh}. \tag{9}$$

The transmission factor $T(\lambda)$ can be calculated for any wavelength by a Taylor series expansion about λ_o,

$$T(\lambda) = T(\lambda_o) + \partial T/\partial\lambda|_{\lambda_o}(\lambda-\lambda_o) + \tfrac{1}{2}\,\partial^2T/\partial\lambda^2|_{\lambda_o}(\lambda-\lambda_o)^2 \ldots \tag{10}$$

Since $\partial T/\partial\lambda = (\partial T/\partial\mu)(\partial\mu/\partial\lambda)$ Equation 10 can be written as

$$T(\lambda) = T(\lambda_o) + \partial T/\partial\mu|_{\mu_o}\ \Delta\mu + \partial^2T/\partial\mu^2|_{\mu_o}\ \Delta\mu^2 + \ldots \qquad (11)$$

where

$$\Delta\mu = \partial\mu/\partial\lambda\ (\lambda-\lambda_o) \cong \mu_o'\ (\lambda/\lambda_o - 1).$$

The attenuation weighted path length $\bar{T}(\lambda)$, necessary for extinction corrections, can also be calculated from $T(\lambda)$ and the derivatives $\partial T/\partial\mu$ and $\partial^2T/\partial\mu^2$ using

$$\bar{T}(\lambda) = - \left[\partial T/\partial\mu|_{\mu_o} + \partial^2T/\partial\mu^2|_{\mu_o}\ \Delta\mu\right] /T(\lambda). \qquad (12)$$

The terms $T(\lambda_o)$, $\partial T/\partial\mu|_{\mu_o}$ and $\partial^2T/\partial\mu^2|_{\mu_o}$ are evaluated by numerical integration.

Hydrogen incoherent scattering

The effective cross section of hydrogen increases with wavelength from the lower (unbound) limit of $\cong$ 20 b to the upper (bound) limit of $\cong$ 80 b over the wavelength range of 0.25 to 4 Å. The particular wavelength dependence was reported by Melkonian[45] for a variety of gases, water and (ℓ) n-butane. In the wavelength range 0.7 to 3.0 Å the cross section for a chemically bonded hydrogen can be represented adequately by

$$\sigma^H \cong 37 + 12\ (\frac{\lambda}{\lambda_o} - 1)\ b \qquad (13)$$

where 1 barn (b) = 10^{-24} cm^2 and λ_o = 1 Å.

Subtracting the wavelength independent Bragg scattering cross section σ^{coh} = 1.8 b yields the hydrogen incoherent scattering cross section.

$$\sigma^{H-incoh} \cong 35.2 + 12(\frac{\lambda}{\lambda_o} - 1) \text{ b}. \qquad (14)$$

The wavelength dependence of the linear attenuation coefficient for any compound can be calculated using Equation 15 if the true absorption and incoherent scattering cross sections are known.

$$\mu(\text{cm}^{-1}) = \frac{1}{V_c}\left(\sum_i(\sigma^{abs} + \sigma^{incoh})\right), \qquad (15)$$

where V_c is the volume of the unit cell and $\sum_i$ runs over all atoms in one unit cell. Evaluation of the resulting expression at a reference wavelength λ_o gives

$$\mu(\lambda) = \mu(\lambda_o) + \mu_o'(\lambda/\lambda_o - 1), \qquad (16)$$

which is of the form applicable for the Taylor series expansion for the transmission factor (Equation 11). The large incoherent scattering cross section for hydrogen will generally dominate in hydrogen containing compounds.

Effective flux

If the thermal neutrons are fully moderated, the incident flux would be the product of a Maxwellian distribution and an effusion rate.[46] Expressed in terms of wavelength

$$\Phi_{\text{incid}} \propto \frac{1}{\lambda^5} e^{-P1/\lambda^2} \tag{17}$$

where P1 is related to the moderator temperature.

Previous work with TOF instruments[47] indicates that the effective detectable flux can be represented by the general four-parameter equation

$$\Phi_{\text{eff}}(\lambda) = K(e^{-P1/\lambda^2}/\lambda^{P3})e^{-P2\lambda}(1 - e^{-P4\lambda}). \tag{18}$$

The expression $e^{-P2\lambda}$ is added to account for the small absorption of the incident beam by Al windows and air, while the expression $(1 - e^{-P4\lambda})$ is a counter efficiency correction. The constant P4 can be determined from the manufacturer's specifications. The expected beam distribution should be Maxwellian (P3 = 3.0).

Obtaining the model

Two methods can be used to obtain structure factors from the white radiation data. The "observed" structure factors can then be phased by the known fragment and a Fourier series calculated. With even approximate amplitudes, the Fourier series will often reveal atoms such as hydrogen which were not found in a previous X-ray analysis.

The first method to obtain F^2's is a simple approximation technique. The low sin(θ) data where only first order scattering is significant is solved for $F_{\underline{1h}}^2$. The contribution of $F_{\underline{1h}}^2$ to the observed intensity streak is subtracted, and the process is repeated for $F_{\underline{2h}}^2$, etc. Since the error in $F_{\underline{nh}}^2$ increases rapidly with n, this method should be terminated when the error in $F_{\underline{nh}}^2$ is of the same magnitude as $F_{\underline{nh}}^2$ itself. An estimate for the extinction correction is easily included in this technique.

A linear least-squares method can be used when the extinction correction is not large. The system of equations (Equation 5) is rewritten here in matrix form as

$$\underline{I} = \underset{\sim}{M} \cdot \left[F^2/d^{*2}\right] . \tag{19}$$

The vector of m observations along one streak is $\underline{I}$, the matrix $\underset{\sim}{M}$ includes flux and transmission factors and $[F^2/d^{*2}]$ is the vector of n unknowns.

For m > n these linear equations are easily solved by a weighted least-squares technique to obtain "observed" structure factors. Along dense reciprocal lattice rows, the calculated high order structure factors may exhibit increasing oscillation about zero. Restricting n to $\leq 2 \sin(\theta_{max})/(1.3d^*)$ has proved adequate to eliminate oscillation. Since only approximate structure factors are necessary to obtain a structural model, this technique should succeed for nearly all problems.

Refining the model

Refinement based on the indirectly "observed" structure factors is possible. However, refinement of the structural model based on observed intensities is more meaningful and does not require determination of accurate structure factors from the data. To perform this refinement a full-matrix least-squares program WIRALS (WhIte RAdiation Least Squares) was written. The quantity minimized is $\Sigma\, w_i (I_i^o - I_i^c)^2$. WIRALS includes refinement of a scale factor, flux parameters, isotropic extinction parameters and atomic coordinates and thermal parameters. WIRALS uses significant portions of ORFLS[13] previously modified to include group refinement. WIRALS corrects the calculated data for extinction and absorption before comparing the calculated and observed intensities. The latter are corrected only for background. All observed data including $I^o < 0$ may be included in the refinement.

Experimental

To experimentally test the "white radiation" method a beam tube of the 5 M.W. Ames Laboratory Research Reactor was temporarily modified to provide a collimated neutron (and gamma) beam at a reactor face. However, due to physical limitations, the diffractometer and biological shielding were located ∿ 5 meters from the reactor face. An evacuated flight tube was placed between the reactor face and the diffractometer to prevent unnecessary air scattering. A secondary collimator at the diffractometer end of the flight tube defined a 3/4 in. diameter beam with a very small divergence angle.

A conventional four-circle E. & A. diffractometer (similar to an X-ray diffractometer) was carefully aligned and surrounded by concrete and paraffin walls for biological shielding. The diffractometer was fully automated using a DATEX controller and the Ames Laboratory SDS-910 real time computer system. The diffractometer was equipped with top/bottom - left/right beam splitters and a shielded BF_3 detector. The main beam was monitored with a U^{235} fission counter. Approximately 1 in 10^4 neutrons is detected by this counter. All diffracted beam counting periods were based on a fixed number of monitor counts.

A spherical NaCl crystal (3.5 mm diameter) was carefully centered and employed for final alignment of the diffractometer. To experimentally confirm that integrated intensities can be obtained by peak height measurements, both peak height and omega scan data were collected. Backgrounds for both intensity measurements were collected at an omega offset of $\pm 2.0°$. As anticipated, the ratio of the peak height to scan intensity data was a constant in the range $10° \leq 2\theta \leq 140°$. This initial study also indicated that much smaller crystals could be used.

The procedure for three-dimensional data collection is as follows. The precise orientation of three non-coplanar Laue reflections is determined using the beam splitters. An orientation matrix is then calculated from the orientation information and calculated reciprocal lattice spacings. During data collection the peak heights of three reflections are periodically remeasured to ensure crystal, flux and electronic stability. For any particular Laue streak with Miller indexes (hkℓ) scattering angles θ are determined by

$$\sin(\theta) = \frac{n\hat{\lambda}}{2d_{\underline{h}}}, \qquad (20)$$

Where n = 1, 2, 3, etc. and $\hat{\lambda}$ = an arbitrary wavelength increment.

The intensity of a Laue streak is measured at each θ determined by Equation 20 ($5° \leq \theta \leq 70°$) for a fixed number of monitor counts. The background is measured on each side of the Laue streak by offsetting omega ($\pm\Delta\Omega$) and counting for the same fixed number of monitor counts. The observed intensity and an expected standard deviation are calculated from the peak height (PH) and the two backgrounds (bg1 and bg2) using

$$I_o = PH - 0.5(bg1 + bg2)$$

and

$$\sigma_I^2 = PH + 0.25(bg1 + bg2) + (0.02\ I_o)^2. \qquad (21)$$

The term $(0.02I_o)^2$ represents an empirical correction for instrument instability. The fact that the wavelength increment $\hat{\lambda}$ can be arbitrarily selected has one important implication. More independent observations are available using this method as compared to a monochromatic beam experiment. This increase in observations provides the possibility of improved refinement of the structural model.

Results

Effective flux

In order to experimentally measure the effective flux, a NaCl crystal (1 x 2 x 2 mm) was mounted on an aluminum rod and carefully aligned with X-rays and neutrons. A total of 155 data points was collected for 55 Laue streaks in one octant of the sphere of reflection using a wavelength increment $\hat{\lambda} = 0.7$ Å and $\Delta\Omega = \pm 2.0°$. Each peak height and background was measured for 10^5 monitor counts ($\sim$ 20 sec).

The linear absorption coefficients for NaCl can be represented[48] by

$$\mu(\lambda) = 0.539 + 0.435\ (\frac{\lambda}{1.08} - 1)\ \text{cm}^{-1}.$$

The scattering lengths $b_{Na} = 3.51$ f[†] and $b_{Cl} = 9.6$ f[49] were used in this study. Assuming a Maxwellian distribution

---

[†] 1 Fermi (f) = 10^{-13}cm.

(P3 = 3.0), a least-squares analysis showed that the data were insensitive to r, the domain radius. The crystal was then assumed to exhibit Type I extinction. To check for any deviation from a Maxwellian distribution, the parameters K, P1, P2, g, B_{Na} and B_{Cl} were refined for various values of P3. The results and estimated standard deviations derived from a least-squares analysis are listed in Table 9. These results indicate that g, B_{Na} and B_{Cl} are independent of the choice of P3. The parameters P1 = 2.41 and P2 = 0.01 for the Maxwellian distribution compare reasonably with anticipated values[‡] of 2.56 and 0.10 respectively. Figure 6 shows the effective flux and incident flux for a Maxwellian distribution as calculated by Equation 18. Table 10 lists the relative wavelength $n\hat{\lambda}$, $I_{obs}/10$ and $I_{calc}/10$ for P3 = 3.0.

The derived thermal parameters $B_{Na} = 1.90 \pm 0.10$ and $B_{Cl} = 1.61 \pm 0.06$ agree within 3σ of reported values.[50] The NaCl study indicates that the effective flux can be adequately described by a simple three-parameter Maxwellian distribution and that meaningful thermal parameters can be obtained using the white radiation method.

[‡] Calculated assuming the moderator is at 100°C and using an estimated path length for neutrons through air and Al windows.

Table 9. Refined parameters as a function of P3 for NaCl

P3	2.5	2.75	3.0	3.25	3.50	Estimated error
K	195.2	192.8	190.7	188.8	187.2	±9
P1	2.26	2.33	2.41	2.48	2.55	±0.03
P2	0.20	0.10	0.01	-0.08	-0.18	±0.03
g	243.3	235.8	228.8	222.2	215.9	±55
B_{Na}	1.89	1.90	1.90	1.91	1.91	±0.10
B_{Cl}	1.61	1.61	1.61	1.61	1.61	±0.06
C^{2a}	0.759	0.748	0.740	0.735	0.732	

$^aC^2 = \Sigma w_i (I_i^o - I_i^c)^2/(NO-NV)$, NO = # observations, NV = # of variables and $w_i = 1/\sigma_i^2$.

Refinement of α - $C_2O_4H_2 \cdot 2H_2O$

The crystal structure of α-oxalic acid dihydrate, hereafter α-POX, was recently studied by neutron diffraction[51] and X-ray diffraction.[52] The study of this structure was expected to be a good test of the white radiation method, especially since extinction and absorption corrections should be important. The sensitivity of the data to atomic parameters and a second determination of the effective flux would also be determined. The lattice constants of Delaplane and Ibers[52], space group $\underline{P2_1/n}$ (Z = 2), $\underline{a}$ = 6.119, $\underline{b}$ = 3.607, $\underline{c}$ = 12.057 Å, β = 106°19', were used in this study.

Figure 6. Incident and effective flux distribution

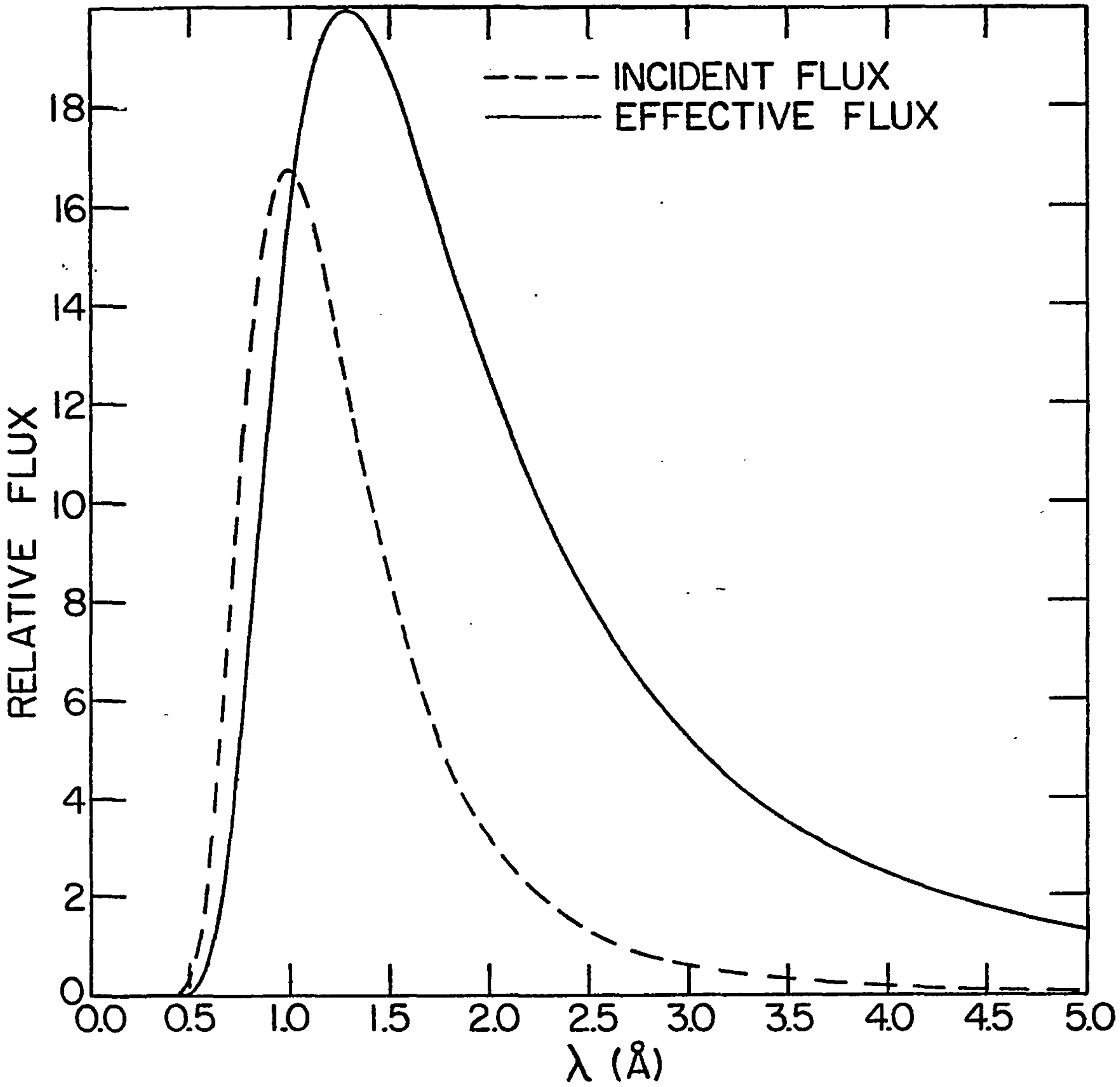
INCIDENT FLUX
EFFECTIVE FLUX
RELATIVE FLUX
0
2
4
6
8
10
12
14
16
18
0.0
0.5
1.0
1.5
2.0
2.5
3.0
3.5
4.0
4.5
5.0
λ (Å)

Table 10. $I_{obs}/10$ and $I_{calc}/10$ for NaCl

n$\hat{\lambda}$	IO	IC	n$\hat{\lambda}$	IO	IC	n$\hat{\lambda}$	IO	IC	n$\hat{\lambda}$	IO	IC	n$\hat{\lambda}$	IO	IC	n$\hat{\lambda}$	IO	IC	n$\hat{\lambda}$	IO	IC	n$\hat{\lambda}$	IO	IC	n$\hat{\lambda}$	IO	IC	n$\hat{\lambda}$	IO	IC	n$\hat{\lambda}$	IO	IC	n$\hat{\lambda}$	IO	IC
*** 2, 0, 01**			1.40	634	631	*** 2, 6, 01**			2.80	224	229	2.10	543	573	0.70	3	2	2.10	99	95	*** 1, 7, 11**			0.70	8	11	0.70	17	18	*** 5, 3, 31**			*** 1, 3, 51**		
0.70	250	263	2.10	389	403	0.70	12	10	3.50	130	141	2.80	334	307	1.40	-13	8	2.80	73	71	0.70	0	2	1.40	70	66	1.40	102	102	0.70	6	7	0.70	0	3
1.40	1343	1372	2.80	232	238	1.40	60	54	*** 4, 0, 21**			3.50	306	287	*** 0, 4, 21**			*** 3, 3, 11**			1.40	11	8	*** 2, 4, 41**			2.10	91	93	1.40	14	12	1.40	17	18
2.10	942	929	3.50	118	135	*** 4, 6, 01**			0.70	36	36	4.20	254	241	0.70	47	35	0.70	8	9	*** 2, 0, 41**			0.70	9	11	2.80	79	72	*** 1, 5, 31**			*** 3, 3, 51**		
2.80	622	612	*** 4, 2, 01**			0.70	5	6	1.40	176	175	4.90	271	204	1.40	173	182	1.40	53	49	0.70	15	14	1.40	66	69	*** 3, 1, 31**			0.70	7	3	0.70	0	2
3.50	409	414	0.70	34	35	1.40	36	30	2.10	98	103	5.60	143	131	2.10	98	99	2.10	39	36	1.40	180	179	*** 0, 6, 41**			0.70	13	9	1.40	17	18	1.40	11	12
4.20	283	283	1.40	100	105	*** 0, 0, 21**			*** 6, 0, 21**			*** 4, 2, 21**			*** 2, 4, 21**			*** 5, 3, 11**			2.10	101	106	0.70	5	6	1.40	63	48	*** 3, 5, 31**			*** 1, 5, 51**		
4.90	128	129	2.10	93	102	0.70	233	249	0.70	10	10	0.70	27	26	0.70	24	26	0.70	2	3	*** 6, 0, 41**			1.40	37	30	2.10	38	36	0.70	3	2	0.70	2	2
*** 0, 2, 01**			*** 6, 2, 01**			1.40	1320	1263	1.40	49	47	1.40	135	136	1.40	134	137	1.40	23	18	0.70	8	6	*** 2, 0, 61**			*** 5, 1, 31**			1.40	12	12	1.40	8	8
0.70	257	263	0.70	7	10	2.10	802	837	*** 0, 2, 21**			*** 3, 1, 11**			*** 4, 4, 21**			*** 1, 5, 11**			1.40	57	50	0.70	10	10	0.70	1	3	*** 1, 1, 51**			*** 1, 1, 71**		
1.40	1375	1370	1.40	57	54	2.80	619	570	0.70	113	118	0.70	14	18	0.70	18	13	0.70	5	5	*** 0, 2, 41**			1.40	94	94	1.40	20	17	0.70	4	5	0.70	1	2
2.10	879	932	*** 2, 4, 01**			3.50	435	404	1.40	614	609	1.40	103	105	1.40	60	56	1.40	32	28	0.70	18	14	*** 4, 0, 61**			*** 2, 4, 61**			1.40	25	20	1.40	7	8
2.80	622	616	0.70	35	35	4.20	313	291	2.10	400	380	2.10	92	94	*** 0, 6, 21**			*** 3, 5, 11**			1.40	175	178	0.70	9	6	0.70	6	6	*** 3, 1, 51**					
3.50	423	415	1.40	198	185	4.90	216	208	2.80	232	219	2.80	81	70	0.70	14	10	0.70	6	5	2.10	97	103	1.40	29	31	1.40	31	30	0.70	2	3			
4.20	257	283	2.10	91	102	*** 2, 0, 21**			3.50	142	136	*** 5, 1, 11**			1.40	97	93	1.40	19	18	*** 2, 2, 41**			*** 0, 2, 61**			*** 1, 3, 31**			1.40	13	10			
4.90	204	190	*** 6, 4, 01**			0.70	99	114	*** 1, 1, 11**			0.70	4	5	*** 1, 3, 11**			*** 5, 5, 11**			0.70	26	26	0.70	7	10	0.70	12	9	*** 5, 1, 51**					
*** 2, 2, 01**			0.70	4	6	1.40	372	384	0.70	54	79	1.40	24	28	0.70	13	18	0.70	3	2	1.40	137	134	1.40	58	54	1.40	51	48	0.70	1	2			
0.70	120	119	1.40	30	30	2.10	336	374	1.40	467	487	*** 7, 1, 11**			1.40	107	106	1.40	3	8	*** 4, 2, 41**			*** 1, 1, 31**			2.10	54	56	1.40	6	8			

A crystal of α-POX (2 mm^3) was mounted on a quartz rod and studied with X-rays to ensure the crystal was of good quality. White radiation neutron data were collected with $\Delta\Omega = \pm 2°$ and $\hat{\lambda} = 0.325$ Å. Since the effective flux is very low for $n\hat{\lambda} = 0.325$ and 0.650 Å, $n\hat{\lambda}$ was initialized at 0.975 Å. A total of 2290 intensities was collected for 681 Laue streaks in the hkℓ and $\bar{h}$kℓ octants. Four intensities were omitted as they were obviously misrecorded. Due to the crude temporary experimental arrangement the background was quite high and only 680 intensities were observed greater than 3 σ_I.

The linear absorption coefficient for α-POX was calculated to be $\mu = 1.66 + 0.53\ (\lambda/\lambda_o - 1)\ cm^{-1}$ at a reference wavelength of 1.08 Å.[48] The range of calculated transmission factors $T(\mu_o)$ was 0.75 to 0.86. The derivatives $\partial T/\partial\mu|_{\mu_o}$ and $\partial^2 T/\partial\mu^2|_{\mu_o}$ were approximately 1/10 and 1/100 of $T(\mu_o)$ respectively. The estimated standard deviations and observed intensities were calculated as described previously.

The α-POX data for each Laue streak were solved for structure factors using the approximation technique. The extinction parameter g from prior data refinement was then used in a least-squares analysis for shifts in F^2's. Using these derived F^2's a Fourier series calculation phased by the reported carbon and oxygen positions[51] clearly revealed all hydrogen atom positions. Subsequent analysis of the high resolution data was best represented by Type I extinction.

In this analysis both KF^2 and g/K were well-determined.

The starting model for least-squares refinement consisted of the atomic parameters reported by Sabine et al.,[51] flux parameters from the NaCl refinement and g = 5000. The scattering lengths used were $b_H = -3.72$ f, $b_C = 6.65$ f and $b_O = 5.77$ f.[49] The 2286 data were refined using anisotropic thermal parameters and a Type I extinction correction until all shifts were less than 0.01 times the corresponding estimated error. Final measures of fit[†] were RI_w $(I > 3\sigma)$ = 0.102 and $RI_w = 0.154$. The final flux parameters were P1 = 2.55 and P2 = 0.06 for P3 = 3.0, which agree quite well with the predicted values of 2.56, 0.1 and 3.0 respectively (moderator at 100°C). The small differences between the flux parameters for α-POX and NaCl (2.41, 0.01, 3.0) are thought to be due to refueling of the reactor between investigations.

The final atomic coordinates are listed in Table 11 along with those reported previously from neutron[51] and X-ray[52] investigations. Similarly, the final thermal parameters are

---

[†] The conventional weighted R-factor is generally based on structure factors, not intensities, and is a poor measure of fit when a large fraction of the data is "unobserved." To avoid confusion the weighted R-factor based on intensities will be $RI_w = \left[\sum_i w_i (I_i^o - I_i^c)^2 / \sum_i w_i (I_i^o)^2\right]^{1/2}$. For comparison with other studies based on observed data RI_w is also reported for only that data with $I > 3\sigma_I$.

Table 11. Fractional positional parameters of all atoms and their standard deviations (All parameters and e.s.d.'s are expressed x 10^4)

		Present work	Neutron[51]	X-ray[52]
	x	854(6)	847(4)	848(1)
01	y	- 574(13)	- 599(6)	- 600(3)
	z	1493(3)	1488(2)	1481(1)
	x	-2193(7)	-2197(3)	-2201(1)
02	y	2328(12)	2310(6)	2305(2)
	z	360(3)	360(2)	361(1)
	x	-4525(8)	-4509(4)	-4512(2)
03	y	6107(15)	6136(6)	6151(2)
	z	1797(5)	1799(2)	1800(1)
	x	- 466(5)	- 452(2)	- 454(2)
Cl	y	599(10)	547(4)	548(3)
	z	509(2)	510(1)	511(1)
	x	262(11)	293(7)	357(20)
H1	y	83(21)	93(12)	- 47(43)
	z	2191(6)	2189(3)	2087(12)
	x	-5742(12)	-5740(7)	-5588(23)
H2	y	6932(23)	6864(13)	6587(45)
	z	1166(6)	1142(3)	1205(16)
	x	-3637(12)	-3599(9)	-3869(31)
H3	y	4450(25)	4447(14)	4508(52)
	z	1510(7)	1508(4)	1584(18)

compared in Table 12. In both cases, the estimated standard deviations were obtained from the least-squares analysis. The atomic parameters determined by the white radiation method essentially all agree within 4σ of the parameters reported by Sabine et al.[51] Since extinction corrections were not applied

Table 12. Thermal parameters[a] of all atoms and their standard deviation (All parameters and e.s.d.'s are expressed x 10^4)

		Present work	Neutron[51]	X-ray[52]
01	β_{11}	194(12)	228(6)	246(3)
	β_{22}	698(42)	827(18)	1019(10)
	β_{33}	34(3)	29(1)	37(1)
	β_{12}	137(21)	143(7)	141(4)
	β_{13}	30(5)	19(2)	26(1)
	β_{23}	29(10)	7(3)	9(2)
02	β_{11}	179(12)	224(6)	226(3)
	β_{22}	772(43)	838(17)	974(10)
	β_{33}	39(3)	32(1)	49(1)
	β_{12}	150(20)	184(7)	158(4)
	β_{13}	35(5)	26(2)	39(1)
	β_{23}	30(10)	7(3)	13(2)
03	β_{11}	204(15)	219(6)	230(4)
	β_{22}	818(51)	829(17)	1007(15)
	β_{33}	40(4)	33(1)	46(1)
	β_{12}	64(23)	69(8)	104(5)
	β_{13}	41(6)	31(2)	35(1)
	β_{23}	7(10)	22(3)	22(2)
C1	β_{11}	124(7)	169(4)	180(3)
	β_{22}	468(32)	462(11)	575(11)
	β_{33}	32(2)	27(1)	42(1)
	β_{12}	24(16)	49(4)	-10(5)
	β_{13}	21(3)	21(1)	22(1)
	β_{23}	6(8)	1(2)	-1(2)
H1	β_{11}	265(20)	285(10)	305(54)
	β_{22}	632(66)	945(29)	1463(183)
	β_{33}	48(6)	45(2)	70(14)
	β_{12}	2(32)	58(14)	-12(78)
	β_{13}	32(8)	32(4)	-76(22)
	β_{23}	0(18)	4(6)	76(43)

---

[a] Form for the anisotropic temperature factor correction is $\exp[-(\beta_{11}h^2 + \beta_{22}k^2 + \beta_{33}l^2 + 2\beta_{12}hk + 2\beta_{13}hl + 2\beta_{23}kl)]$.

Table 12 (Continued)

		Present work	Neutron[51]	X-ray[52]
H_2	β_{11}	251(22)	314(12)	281(59)
	β_{22}	1028(86)	1083(35)	1868(238)
	β_{33}	44(6)	50(3)	96(17)
	β_{12}	150(38)	105(17)	200(86)
	β_{13}	11(10)	24(4)	51(27)
	β_{23}	99(19)	47(7)	15(49)
H3	β_{11}	287(25)	343(13)	608(91)
	β_{22}	1159(91)	1097(40)	1134(252)
	β_{33}	96(8)	79(3)	172(25)
	β_{12}	240(43)	126(19)	227(110)
	β_{13}	95(12)	66(5)	-75(37)
	β_{23}	-101(24)	15(9)	210(63)

in the previous neutron study, the agreement of parameters is considered excellent. The observed and calculated intensities are listed in Table 13. The extinction constant g was refined to $12.7 \times 10^3 \pm 0.8 \times 10^3$. The successful refinement of α-POX indicates that omission of corrections for inelastic scattering and multiple Bragg scattering was justified.

Discussion

In this section methods for improving the experimental design and further applications of the white radiation method are discussed.

Table 13. I_{obs} and I_{calc} for α-POX

[illegible]	IO	IC	[illegible]	IO	IC	[illegible]	IO	IC	[illegible]	IO	IC	[illegible]	IO	IC	[illegible]	IO	IC	[illegible]	IO	IC	[illegible]	IO	IC	[illegible]	IO	IC	[illegible]	IO	IC	[illegible]	IO	IC	[illegible]	IO	IC	[illegible]	IO	IC
[illegible]	[illegible]	[illegible]	[illegible]	[illegible]	[illegible]	[illegible]	[illegible]	[illegible]	[illegible]	[illegible]	[illegible]	[illegible]	[illegible]	[illegible]	[illegible]	[illegible]	[illegible]	[illegible]	[illegible]	[illegible]	[illegible]	[illegible]	[illegible]	[illegible]	[illegible]	[illegible]	[illegible]	[illegible]	[illegible]	[illegible]	[illegible]	[illegible]	[illegible]	[illegible]	[illegible]	[illegible]	[illegible]	[illegible]

Table 13 (Continued)

nλ	Io	Ic
(-4, 1, 4)		
0.975	-1	5
1.300	33	7
1.625	-9	7
(-7, 1, 4)		
0.975	72	10
1.300	84	14
(-8, 1, 4)		
0.975	101	19
1.300	1	21
(-1, 2, 4)		
0.975	746	818
1.300	936	968
1.625	774	720
1.950	567	444
2.275	379	265
2.600	338	190
(-3, 2, 4)		
0.975	84	5
1.300	94	8
1.625	-30	11
1.950	18	19
2.275	40	16
(-5, 2, 4)		
0.975	11	6
1.300	-26	11
1.625	55	10
(-7, 2, 4)		
0.975	67	10
1.300	14	14
(-1, 3, 4)		
0.975	-35	30
1.300	6	40
1.625	92	34
1.950	2	26
(-2, 3, 4)		
0.975	194	189
1.300	251	255
1.625	179	175
1.950	116	104
(-3, 3, 4)		
0.975	-32	52
1.300	122	48
1.625	32	54
(-4, 3, 4)		
1.300	-3	0
1.625	-50	0
(-5, 3, 4)		
0.975	24	8
1.300	25	11
(-8, 1, 4)		
0.975	101	19
1.300	1	21
(-1, 2, 4)		
0.975	744	818
1.300	936	968
1.625	794	710
1.950	567	444
2.275	379	265
2.600	338	190
(-3, 2, 4)		
0.975	84	5
1.300	94	8
1.625	-30	11
1.950	18	19
2.275	40	16
(-5, 2, 4)		
0.975	11	6
1.300	-26	11
1.625	55	10
(-7, 2, 4)		
0.975	67	10
1.300	14	14
(-1, 3, 4)		
0.975	-35	30
1.300	6	40
1.625	52	36
1.950	2	26
(-2, 3, 4)		
0.975	194	189
1.300	251	255
1.625	179	175
1.950	114	104
(-3, 3, 4)		
0.975	-32	52
1.300	122	48
1.625	32	54
(-4, 3, 4)		
0.975	-39	0
1.300	-2	0
1.625	-50	0
(-5, 3, 4)		
0.975	26	6
1.300	25	11
(-6, 3, 4)		
0.975	32	2
1.300	-8	2
(-1, 4, 4)		
0.975	41	57
1.300	-29	73
(-3, 4, 4)		
0.975	-23	15
1.300	-22	20
(-5, 4, 4)		
0.975	-28	0
1.300	33	0
(-1, 0, 5)		
0.975	6382	6615
1.300	4551	4714
1.625	3454	3483
1.950	2626	2497
2.275	1763	1891
2.600	1567	1541
2.925	1309	1309
3.250	1027	1128
3.575	851	944
3.900	765	813
4.225	505	457
(-4, 0,10)		
0.975	172	104
1.137	116	135
1.300	202	143
1.462	198	137
1.625	96	126
1.787	111	112
(-3, 0, 5)		
0.975	1360	1344
1.300	1565	1527
1.625	1076	1129
1.950	798	747
2.275	559	484
2.600	376	315
2.925	305	203
(-8, 0,10)		
0.975	-11	31
1.137	43	60
1.300	85	42
(-7, 0, 5)		
0.975	-29	0
1.300	10	0
(-1, 1, 5)		
0.975	782	831
1.300	945	819
1.625	895	769
1.950	782	709
2.275	574	627
2.600	494	531
2.925	512	436
3.250	356	341
3.575	263	261
(-2, 1, 5)		
0.975	2931	2437
1.300	3153	2672
1.625	2241	1826
1.950	1309	1104
2.275	832	704
2.600	451	517
2.925	444	354
3.250	323	242
(-3, 1, 5)		
0.975	173	126
1.300	138	169
1.625	79	154
1.950	135	132
2.275	34	113
2.600	96	97
(-4, 1, 5)		
0.975	476	518
1.300	636	629
1.625	497	481
1.950	355	324
2.275	210	201
(-5, 1, 5)		
0.975	74	49
1.300	29	47
1.625	40	58
1.950	48	43
(-6, 1, 5)		
0.975	-41	17
1.300	-15	24
1.625	-10	21
(-7, 1, 5)		
0.975	41	119
1.300	83	136
(-8, 1, 5)		
0.975	31	0
1.300	27	0
(-2, 2, 5)		
0.975	97	143
1.300	130	187
1.625	181	192
1.950	90	106
2.275	94	89
2.600	18	42
(-3, 2, 5)		
0.975	29	4
1.300	56	6
1.625	69	6
(-4, 5, 4)		
0.975	-39	0
(-2, 2, 5)		
1.950	-46	5
2.275	-13	5
(-3, 2, 5)		
0.975	997	876
1.300	1013	903
1.625	875	866
1.950	520	418
2.275	296	238
(-4, 2, 5)		
0.975	11	0
1.300	10	0
1.625	-12	0
1.950	-82	1
(-5, 2, 5)		
0.975	164	109
1.300	138	143
1.625	140	118
(-6, 2, 5)		
0.975	91	81
1.300	95	108
(-7, 2, 5)		
0.975	-19	10
1.300	19	13
(-1, 3, 5)		
0.975	6	2
1.300	-8	3
1.625	-54	8
(-2, 3, 5)		
0.975	59	133
1.300	94	132
1.625	36	102
(-3, 3, 5)		
0.975	-29	38
1.300	-72	50
1.625	37	41
(-4, 3, 5)		
0.975	135	102
1.300	149	128
1.625	97	100
(-5, 3, 5)		
0.975	3	70
1.300	31	92
(-6, 3, 5)		
0.975	37	14
1.300	35	20
(-1, 4, 5)		
0.975	44	17
1.300	39	22
(-2, 4, 5)		
0.975	16	31
1.300	-1	40
(-3, 4, 5)		
0.975	26	2
1.300	51	2
(-4, 4, 5)		
0.975	-78	1
1.300	27	1
(-5, 4, 5)		
0.975	-38	2
1.300	-62	2
(-2, 0,12)		
0.975	277	367
1.137	242	304
1.300	291	307
1.462	284	278
1.625	210	233
1.787	173	183
(-10, 0,12)		
0.975	-27	0
(-1, 1, 6)		
0.975	73	101
1.300	92	137
1.625	126	127
1.950	106	110
2.275	13	93
2.600	111	77
2.925	111	62
(-2, 1, 6)		
0.975	27	56
1.300	117	75
1.625	128	69
1.950	86	91
2.275	28	40
2.600	15	31
2.925	120	25
(-3, 1, 6)		
0.975	30	15
1.300	114	102
1.625	99	96
1.950	135	83
2.275	100	73
2.600	92	61
(-4, 1, 6)		
0.975	218	196
1.300	267	261
1.625	260	229
1.950	161	185
2.275	131	143
(-5, 1, 6)		
0.975	519	428
1.300	565	527
1.625	403	410
1.950	363	266
(-6, 1, 6)		
0.975	-6	0
1.300	39	0
1.625	-96	1
(-7, 1, 6)		
0.975	42	80
1.300	110	107
(-8, 1, 6)		
0.975	-18	0
1.300	-58	0
(-1, 2, 6)		
0.975	256	202
1.300	242	260
1.625	191	206
1.950	156	119
2.275	-10	84
(-3, 2, 6)		
0.975	259	153
1.300	206	196
1.625	118	153
1.950	116	106
(-5, 2, 6)		
0.975	-39	0
1.300	31	11
1.625	44	10
(-7, 2, 6)		
0.975	-46	6
1.300	30	8
(-1, 3, 6)		
0.975	-23	1
1.300	30	1
1.625	-54	1
(-2, 3, 6)		
0.975	382	352
1.300	483	410
1.625	318	279
(-4, 3, 6)		
0.975	33	1
1.300	-29	1
1.625	73	1
(-5, 3, 6)		
0.975	-29	32
1.300	59	43
(-1, 4, 6)		
0.975	238	84
1.300	76	106
(-3, 4, 6)		
0.975	16	27
1.300	-10	35
(-1, 0, 7)		
0.975	-6	47
1.300	18	65
1.625	72	63
1.950	80	59
2.275	51	55
2.600	37	50
2.925	-1	45
(-4, 0,14)		
0.975	70	19
1.137	6	25
1.300	0	26
1.462	-20	25
(-5, 0, 7)		
0.975	32	5
1.300	13	8
1.625	44	9
1.950	46	11
2.275	-22	12
2.600	6	12
(-8, 0,14)		
0.975	-1	2
1.137	-19	2
(-9, 0, 7)		
0.975	841	782
1.300	959	912
1.625	673	671
1.950	480	407
(-1, 1, 7)		
0.975	681	623
1.300	801	755
1.625	587	569
1.950	412	369
2.275	292	278
2.600	120	117
(-2, 1, 7)		
0.975	-7	0
1.300	26	5
1.625	8	24
1.950	37	45
2.275	81	58
2.600	63	61
(-3, 1, 7)		
0.975	-36	6
1.300	-30	8
1.625	27	8
1.950	36	7
2.275	-18	7
(-4, 1, 7)		
0.975	526	498
1.300	667	592
1.625	473	451
1.950	315	296
(-5, 1, 7)		
0.975	-10	28
1.300	5	38
1.625	69	35
(-6, 1, 7)		
0.975	100	206
1.300	255	266
1.625	227	200
(-7, 1, 7)		
0.975	172	85
1.300	164	113
(-8, 1, 7)		
0.975	67	9
1.300	-5	4
(-1, 2, 7)		
0.975	163	252
1.300	294	318
1.625	305	267
1.950	136	160
(-2, 2, 7)		
0.975	257	173
1.300	207	221
1.625	215	173
1.950	130	116
(-3, 2, 7)		
0.975	299	354
1.300	390	421
1.625	363	313
1.950	193	200
(-4, 2, 7)		
0.975	-11	26
1.300	104	85
1.625	56	90
(-5, 2, 7)		
0.975	62	48
1.300	79	64
1.625	-21	54
(-6, 2, 7)		
0.975	30	15
1.300	69	21
(-7, 2, 7)		
0.975	49	6
1.300	19	6
(-1, 3, 7)		
0.975	166	95
1.300	74	121
1.625	40	93
(-2, 3, 7)		
0.975	-21	0
1.300	4	0
1.625	61	9
(-3, 3, 7)		
0.975	89	85
1.300	61	107
1.625	51	86
(-4, 3, 7)		
0.975	55	13
1.300	-1	18
(-5, 3, 7)		
0.975	-101	2
1.300	41	3
(-6, 3, 7)		
0.975	-17	3
1.300	41	4
(-1, 4, 7)		
0.975	2	0
1.300	-44	0
(-2, 4, 7)		
0.975	15	21
1.300	52	27
(-3, 4, 7)		
0.975	-65	12
1.300	16	15
(-4, 4, 7)		
0.975	-12	1
1.300	44	1
(-2, 0,14)		
0.975	119	114
1.137	190	142
1.300	79	142
(-6, 0,14)		
0.975	-22	72
1.137	15	90
(-1, 1, 8)		
0.975	599	536
1.300	711	648
1.625	494	486
1.950	347	315
2.275	167	191
(-2, 1, 8)		
0.975	358	356
1.300	519	467
1.625	441	381
1.950	360	316
2.275	209	257
(-3, 1, 8)		
0.975	58	19
1.300	52	27
1.625	60	27
1.950	23	26
2.275	-22	24
(-4, 1, 8)		
0.975	172	112
1.300	156	140
1.625	101	123
1.950	52	86
(-5, 1, 8)		
0.975	31	8
1.300	14	11
1.625	-12	12
(-6, 1, 8)		
0.975	62	35
1.300	127	40
1.625	91	41
(-7, 1, 8)		
0.975	-121	2
1.300	-113	3
(-8, 1, 8)		
0.975	-61	3
1.300	2	8
(-1, 2, 8)		
0.975	117	116
1.300	96	149
1.625	143	120
1.950	81	80
(-3, 2, 8)		
0.975	-21	19
1.300	72	20
1.625	79	20
1.950	-57	14
(-5, 2, 8)		
0.975	37	3
1.300	54	5
1.625	-47	6
(-7, 2, 8)		
0.975	79	32
1.300	75	43
(-1, 3, 8)		
0.975	62	11
1.300	55	15
1.625	-7	15
(-2, 3, 8)		
0.975	21	0
1.300	-66	0
1.625	33	0
(-3, 3, 8)		
0.975	62	1
1.300	24	2
1.625	-19	1
(-4, 3, 8)		
0.975	7	31
1.300	101	41
(-5, 3, 8)		
0.975	-100	1
1.300	-97	1
(-6, 3, 8)		
0.975	-4	8
1.300	-19	10
(-1, 4, 8)		
0.975	-30	2
1.300	67	3
(-3, 4, 8)		
0.975	-109	0
1.300	-16	0
(-1, 0, 9)		
0.975	707	765
1.300	988	820
1.625	528	544
1.950	215	248
2.275	180	171
(-4, 0,18)		
0.975	29	2
1.137	66	3
(-8, 0,18)		
0.975	17	2
(-5, 0, 9)		
0.975	26	17
1.300	78	50
1.625	97	41
(-4, 3, 9)		
0.975	27	11
1.300	0	15
(-9, 3, 9)		
0.975	20	32
1.300	49	43
(-1, 4, 9)		
0.975	-51	43
1.300	-20	53
(-2, 4, 9)		
0.975	12	7
1.300	61	5
(-3, 4, 9)		
0.975	41	3
1.300	30	4
(-2, 0,20)		
0.975	-6	16
(-6, 0,20)		
0.975	1	4
(-1, 1,10)		
0.975	484	512
1.300	616	589
1.625	367	430
1.950	279	251
(-2, 1,10)		
0.975	19	54
1.300	57	72
1.625	124	67
1.950	11	44
(-3, 1,10)		
0.975	247	257
1.300	279	323
1.625	244	257
1.950	125	132
(-4, 1,10)		
0.975	10	27
1.300	40	49
1.625	90	35
(-5, 1,10)		
0.975	48	15
1.300	-37	21
1.625	-39	19
(-6, 1,10)		
0.975	51	69
1.300	85	92
(-7, 1,10)		
0.975	0	27
1.300	-25	30
(-1, 2,10)		
0.975	20	9
1.300	98	13
1.625	5	12
(-3, 2,10)		
0.975	93	26
1.300	-30	36
1.625	43	30
(-5, 2,10)		
0.975	39	27
1.300	-37	36
(-7, 2,10)		
0.975	-16	2
1.300	-13	3
(-1, 3,10)		
0.975	56	26
1.300	70	36
(-2, 3,10)		
0.975	-17	8
1.300	32	11
(-3, 3,10)		
0.975	18	61
1.300	93	53
(-4, 3,10)		
0.975	16	103
1.300	167	129
(-5, 3,10)		
0.975	0	11
1.300	10	15
(-1, 4,10)		
0.975	11	15
1.300	-7	19
(-1, 0,11)		
0.975	968	944
1.300	1177	1048
1.625	744	761
1.950	476	424
(-4, 0,22)		
0.975	25	0
(-3, 0,11)		
0.975	119	90
1.300	173	120
1.625	76	100
(-9, 0,11)		
0.975	15	0
1.300	16	1
1.625	-30	2
(-7, 0,11)		
0.975	207	235
1.300	207	282
(-1, 1,11)		
0.975	285	222
1.300	471	381
1.625	229	210
(-2, 1,11)		
0.975	415	376
1.300	445	442
1.625	255	174
(-3, 1,11)		
0.975	46	62
1.300	160	56
1.625	105	48
(-4, 1,11)		
0.975	56	2
1.300	56	3
1.625	-49	1
(-5, 1,11)		
0.975	46	40
1.300	115	55
(-6, 1,11)		
0.975	175	104
1.300	97	134
(-7, 1,11)		
0.975	46	47
1.300	76	56
(-1, 2,11)		
0.975	4	17
1.300	36	15
1.625	45	13
(-2, 2,11)		
0.975	145	135
1.300	95	215
1.625	196	156
(-3, 2,11)		
0.975	10	56
1.300	125	73
1.625	55	60
(-4, 2,11)		
0.975	150	109
1.300	131	141
(-5, 2,11)		
0.975	98	112
1.300	250	145
(-6, 2,11)		
0.975	107	109
1.300	202	139
(-1, 3,11)		
0.975	-26	5
1.300	-15	5
(-2, 3,11)		
0.975	0	0
1.300	-13	0
(-3, 3,11)		
0.975	62	108
1.300	131	131
(-4, 3,11)		
0.975	67	20
1.300	35	26
(-5, 3,11)		
0.975	56	99
1.300	135	124
(-1, 1,12)		
0.975	-30	9
1.300	-16	12
1.625	-24	10
(-2, 1,12)		
0.975	88	88
1.300	96	114
1.625	90	92
(-3, 1,12)		
0.975	90	47
1.300	-13	44
1.625	90	55
(-4, 1,12)		
0.975	22	0
1.300	46	1
1.625	-95	0
(-5, 1,12)		
0.975	45	25
1.300	6	35
(-6, 1,12)		
0.975	56	71
1.300	67	96
(-7, 1,12)		
0.975	97	75
1.300	55	97
(-1, 2,12)		
0.975	67	4
1.300	-32	5
(-3, 2,12)		
0.975	-22	19
1.300	80	26
(-5, 2,12)		
0.975	61	58
1.300	107	77
(-1, 3,12)		
0.975	-10	1
1.300	49	1
(-2, 3,12)		
0.975	-1	1
1.300	-21	1
(-4, 3,12)		
0.975	19	71
1.300	95	89
(-1, 0,13)		
0.975	111	9
1.300	20	12
(-3, 0,13)		
0.975	-44	1
1.300	45	1
1.625	4	2
(-5, 0,13)		
0.975	111	78
1.300	71	104
(-7, 0,13)		
0.975	49	55
1.300	94	71
(-1, 1,13)		
0.975	62	1
1.300	21	1
(-2, 1,13)		
0.975	-71	4
1.300	31	4
1.625	-55	4
(-3, 1,13)		
0.975	107	104
1.300	172	136
(-4, 1,13)		
0.975	35	36
1.300	29	46
(-5, 1,13)		
0.975	-10	0
1.300	61	1
(-6, 1,13)		
0.975	35	5
1.300	-25	5
(-1, 2,13)		
0.975	-41	17
1.300	70	26
(-2, 2,13)		
0.975	79	11
1.300	25	14
(-3, 2,13)		
0.975	16	37
1.300	161	49
(-4, 2,13)		
0.975	12	16
1.300	19	22
(-5, 2,13)		
0.975	-12	17
1.300	31	23
(-1, 3,13)		
0.975	33	4
1.300	56	4
(-2, 3,13)		
0.975	-57	0
1.300	-26	3
(-3, 3,13)		
0.975	-9	4
1.300	-50	7
(-1, 1,14)		
0.975	35	3
1.300	29	4
(-2, 1,14)		
0.975	94	59
1.300	110	77
(-3, 1,14)		
0.975	8	4
1.300	22	5
(-4, 1,14)		
0.975	-59	2
1.300	-84	3
(-5, 1,14)		
0.975	-18	2
1.300	3	2
(-6, 1,14)		
0.975	-29	31
1.300	-17	41
(-1, 2,14)		
0.975	29	49
1.300	77	65
(-3, 2,14)		
0.975	-30	8
1.300	3	11
(-5, 2,14)		
0.975	47	9
1.300	-71	12
(-1, 0,15)		
0.975	115	120
1.300	90	152
(-1, 1,15)		
0.975	106	67
1.300	-69	86
(-2, 1,15)		
0.975	178	147
1.300	110	190
(-3, 1,15)		
0.975	2	8
1.300	-18	11
(-4, 1,15)		
0.975	117	131
1.300	157	161
(-5, 1,15)		
0.975	61	10
1.300	-66	14
(-1, 2,15)		
0.975	2	7
1.300	10	9
(-2, 2,15)		
0.975	17	22
1.300	8	29
(-3, 2,15)		
0.975	26	18
1.300	29	24
(-2, 1,16)		
0.975	-12	6
1.300	-101	0
(-3, 1,16)		
0.975	118	61
1.300	82	70
(-4, 1,16)		
0.975	59	20
1.300	-62	26

Experimental improvements

Air scattering of the incident beam is the primary source of background. The temporary experimental design used in these studies can be readily modified to use a smaller beam cross section and smaller counter aperture. This modification considerably reduces the background. The smaller counter aperture will also improve resolution of the diffractometer. Background measurements with an omega offset of ±2° are satisfactory if the reciprocal lattice is not too dense. However, a background measurement in the proximity of a neighboring Laue streak must be avoided. An omega offset of ±1° is easily obtainable and should suffice for most problems.

In the new experimental arrangement, the incident beam will have a variable cross section up to 5 mm and an included divergence angle up to 1°. The sample crystal will be centered only 1 m from the reactor face. Improved collimation design and shielding materials should further reduce the background. The incident flux is predicted to be an order of magnitude more intense and the peak-to-background ratio is to be increased by a factor of five.

The presence of long wavelength (> 2 Å) neutrons in the incident beam contributes to several difficulties in data collection and analysis. Since air scattering increases with wavelength, the background can be decreased if the long wavelength neutron flux is reduced. Both extinction and absorption corrections also increase with increasing wavelength. To partially eliminate these complications a wavelength selective filter is necessary.

A convenient filter is an Eu-Al alloy (6.5 wt % Eu). The theoretical transmission factors based on the Eu cross section through a 1 mm foil are 0.90 at 1 Å and 0.49 at 3 Å. To test such a foil 420 data points were collected along one Laue streak of NaCl with the incident beam filtered (f) and unfiltered (uf). Least-squares analysis determined both $\Phi(\lambda)_f$ and $\Phi(\lambda)_{uf}$. The RI_w were 0.050 and 0.057 respectively. The calculated ratio of $\Phi(\lambda)_f$ to $\Phi(\lambda)_{uf}$ is 0.95 at 1 Å and 0.52 at 3 Å. These results indicate that use of this filter should improve both data collection and analysis.

Further applications

The application of the white radiation method to other scattering problems is also possible. For example, the study of magnetic ordering is feasible with this technique. In order to demonstrate this, a 2 x 2 x 25 mm Cr crystal was mounted on our single-crystal diffractometer. The magnetic lattice of antiferromagnetic Cr has been reported[53] to be $(28)^3$ times larger than the bcc nuclear lattice. The magnetic satellites about the 100 reciprocal lattice point were calculated to occur at $\Delta\Omega = \pm 2.1°$. Partial overlap of nuclear and magnetic scattering was anticipated due to the 1.7° resolution of our diffractometer.

Omega scans across the 100 Laue spot are reproduced in Figures 7a and 7b for scattering angles of 12.5° and 20.0°. Each observation was based on 10^5 monitor counts ($\sim$ 20 sec). At $\theta = 20°$ the Bragg diffraction from the 200 nuclear planes begins to obscure the magnetic satellites. Our measurements indicate that magnetic scattering can indeed be studied efficiently using the white radiation technique.

If reciprocal space can be accurately mapped by unfolding the observed intensity streak, then inelastic scattering, liquid and powder diffraction studies could be performed using the white radiation method. Least-squares techniques using auxiliary conditions are currently being studied as means to achieve this unfolding. Thermal energy total cross sections can also be measured using a polychromatic beam transmitted through the sample and analyzed via a conventional crystal. Compared to time-of-flight techniques much higher intensities should be obtained.

Conclusion

The successful structure refinement of α-POX using the white radiation data demonstrates that this new method is a dramatic development in single-crystal neutron diffraction techniques. No other method developed or proposed can realize the efficient use of the thermal neutron spectrum obtained by this method. The large increase in efficiency over

Figure 7. Antiferromagnetic chromium 100 magnetic satellites
a) θ = 12.5° b) θ = 20.0°

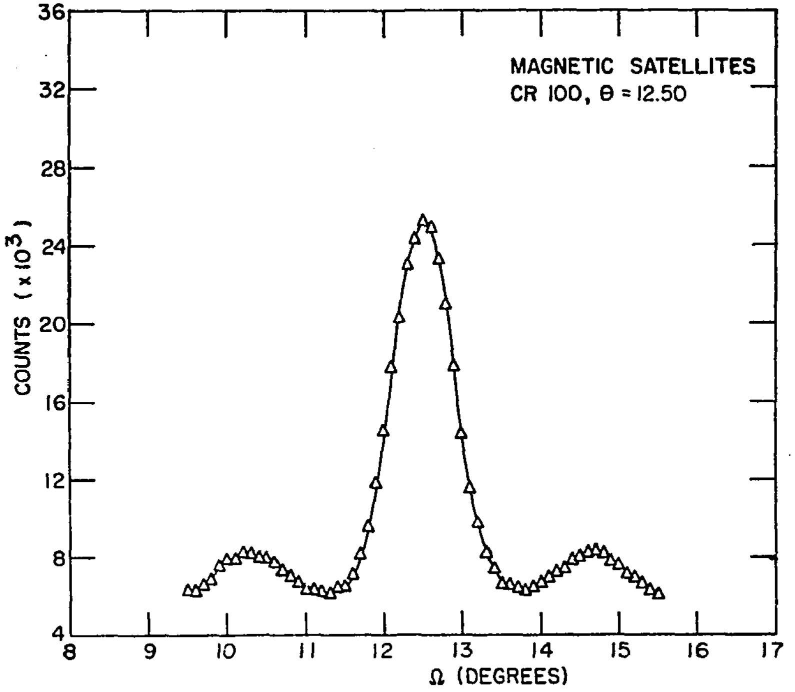
MAGNETIC SATELLITES
CR 100, θ = 12.50
COUNTS (x 10³)
4
8
12
16
20
24
28
32
36
8
9
10
11
12
13
14
15
16
17
Ω (DEGREES)

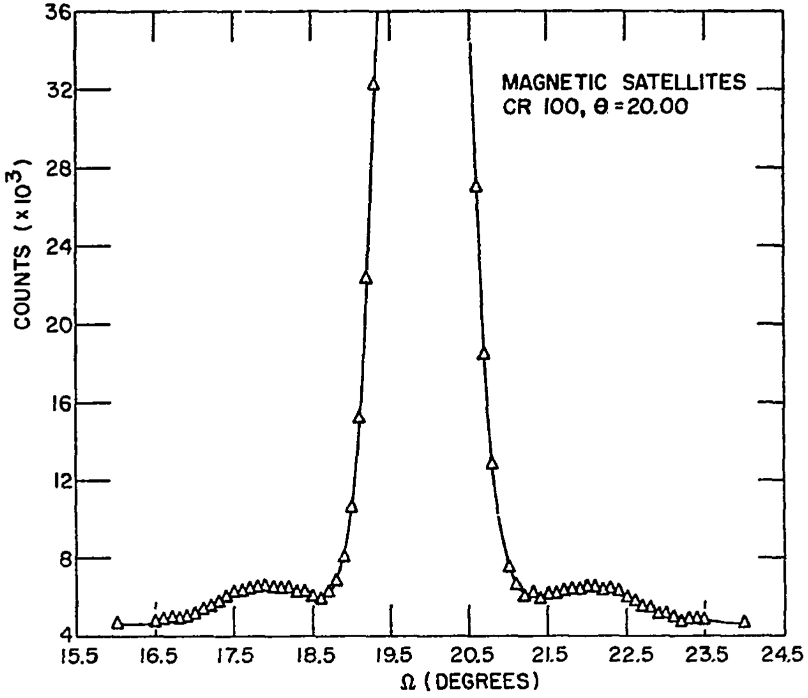
MAGNETIC SATELLITES
CR 100, θ = 20.00
COUNTS (x 10³)
4
8
12
16
20
24
28
32
36
15.5
16.5
17.5
18.5
19.5
20.5
21.5
22.5
23.5
24.5
Ω (DEGREES)

conventional methods enables the experimenter to study much smaller crystals at faster data rates without sacrificing experimental precision. This reduction in necessary crystal size permits a much wider variety of compounds to be studied by neutron diffraction.

CRYSTALLOGRAPHY AND THE COMPUTER

Introduction

The evolution of crystallography in recent years has closely paralleled the rapid development of high speed computers. The Proceedings of the 1969 International Summer School on Crystallographic Computing[54] clearly reveal the importance of computers in crystallography. For example, a single crystal structure determination may include the following computer assisted calculations: 1) data reduction; 2) statistical tests; 3) three-dimensional Fourier series; 4) Patterson and/or symmetry map superpositions; 5) structure-factor least-squares refinement; 6) crystallographic drawings; and 7) bond distances and angles with associated errors. Although these calculations are usually performed employing a large computer such as Iowa State University's IBM 360/65, the birth of 'mini' computers has also been important in expanding the range of problems capable of being studied. These 'mini' computers, either in a dedicated or time sharing environment, provide automation and 24 hour operation of film readers and diffractometers. Since computation is an integral part of modern crystallography, the author has attempted to expand and update the crystallographic computing library of Iowa State University and the crystallographic community. Two major systems of programs were developed in addition to a number of secondary programs. The major systems of programs are discussed below, while the minor programs are summarized. Details on automation of the Datex interfaced E. & A. diffractometer used in the white radiation experiments are omitted due to the complex and continually changing program system.

A System of Programs for Generalized Superpositions

The superposition technique[55] was introduced to locate one image of an N-atom structure by deconvolution of the N images of the Patterson. In practice, this process consists of performing a superposition of several shifted Patterson maps on an unshifted Patterson map. Each shift vector must be a vector from a given atom to any of the other N-1 atoms in the same image. Generalization of the base map to include symmetry maps[56,57] and pseudo electron density maps extends the usefulness of the superposition technique. A generalized definition of a superposition map is

$$\underline{S}(\underset{\sim}{u}) = \mathrm{MIN}\{\mathrm{MAP1}(\underset{\sim}{u}),\ w_1*\mathrm{MAP2}(\underset{\sim}{u}-\underset{\sim}{s}_1),\ w_2*\mathrm{MAP2}(\underset{\sim}{u}-\underset{\sim}{s}_2),\ldots\}\ ,$$

where MAP2 = Patterson map, MAP1 = Patterson, symmetry, or pseudo electron density map, $\underset{\sim}{s}_i$ = shift vector and w_i = weighting factor.

A system of programs to efficiently calculate the superposition map $\underline{S}(\underset{\sim}{u})$ has been written in FORTRAN IV for the IBM 360/65 computer and consists of three programs: GEN, SYMM, and ALS. The first program is used to generate the data set of appropriate format for the other two programs using the output of a Patterson program.[58] The second program, SYMM, is used if a symmetry map is to be calculated. The third program, ALS, performs the superposition and was written with four requirements in mind: (1) small computer core allocation, (2) high speed execution, (3) generalized superpositions using the minimum function and (4) weighting, origin shift, and multiple superposition options.

To satisfy these four requirements, ALS calculates all superpositions for a given layer of the resultant superposition map before proceeding to the next layer. With this technique, storage for only two 2-dimensional arrays is required. Storage requirements are further reduced by using two-byte words for each point in the base and Patterson maps. The symmetry unique regions of both maps are stored on magnetic disk packs in the direct access mode; each layer is randomly accessible. Input delays are reduced by appropriate buffering and use of the direct access FIND statement which permits overlapping of disk access and computation. The calculation of eight superpositions of a monoclinic Patterson on a symmetry map of grid 31*43*23 required 64K bytes storage and 100 seconds CPU time on our computer. Further details concerning the superposition system of programs are given in the AEC Report IS-2210.[59]

ALFF and a Comparison of the Fast and Trigonometric Fourier Algorithms

The Fourier series calculation is frequently used throughout the process of crystal structure analysis. Calculation of the Patterson function, E-maps and electron density maps are used in nearly all structure determinations. The Fourier map is the basis for elucidation of the structure of large biological molecules. In addition, Fourier series have recently been employed to link direct and Patterson methods,[60] to test structural fragments[61] and to extend protein phases.[62] For such methods to be practicable, it is necessary to be able to calculate Fourier series very rapidly. The Cooley-Tukey fast Fourier (FF) algorithm has been reported[63-65] to be more efficient than other Fourier algorithms, including the factored trigonometric Fourier (TF) algorithm[66] currently used nearly exclusively by crystallographers.

The program ALFF[67] was written to evaluate the fast Fourier algorithm for crystallographic Fourier series calculations. This program employs the IBM subroutine FFTM[68] which calculates multi-dimensional Fourier series. To enable nearly any size map to be calculated by ALFF, the 3-dimensional synthesis is factored into a series of 2-dimensional and 1-dimensional syntheses. Intermediate data is saved and retrieved from a random access disk data file. This factoring technique enables large maps (e.g. 64x64x64 grid points) to be calculated in less than 128K bytes of main core and can reduce computing time in cases where the full map is not required.

Further details concerning this program and the related programs ALFFT, ALFFDP, ALFFPROJ and FRIEDEL are given in the AEC Report IS-2625.[67]

Numerous comparisons concerning details of the Fourier algorithms are possible. However, it is most logical to compare GO step central processing (CPU) times of the fast Fourier program and programs recently written at this laboratory based on the TF algorithm. The programs compared are: ALFF, a completely general FF program written in PL/1; ALF,[58] a TF program for triclinic, monoclinic and orthorhombic space groups written in PL/1; and HEX, a FORTRAN IV TF program written by this author specifically for the centrosymmetric space group $P6_3/mmc$. All three programs employ the factoring technique[66] and were written for the Iowa State University IBM 360/65 computer. Both PL/1 programs were compiled by the F level compiler with options 'NOSTMT, OPT = 2' employed and the prefix conditions SUBRG,STRG omitted. Thus the GO step CPU times only reflect differences in the respective Fourier algorithms. The program HEX was compiled by the FORTH (OPT = 2) compiler.

For the four comparisons to be presented, the map printing was suppressed in all programs (ALFF contains a very rapid technique which greatly reduces the CPU time required for map printing). All three programs employ Friedel's law in their respective algorithm and use identical precision (32 bits/word) throughout their calculations.

Table 14. Data for four example problems

Program	Grid x y z	Map fraction calculated	CPU time (seconds)	Region size (in 1024 bytes)
Example 1 $P\bar{1}$ 3617 unique data a = 10.93, b = 14.11, c = 9.78, α = 104.8, β = 107.7, γ = 99.9				
ALF	34 x 34 x 32	$1 \times 1 \times \frac{1}{2}$	70.6	100
ALFF	32 x 32 x 32	$1 \times 1 \times \frac{1}{2}$	15.1	90
Example 2 $P2_1/c$ 3258 unique data a = 19.22, b = 13.47, c = 19.50, β = 111.89				
ALF	62 x 30 x 64	$1 \times \frac{1}{2} \times \frac{1}{2}$	322.2	112
ALFF	64 x 32 x 64	$1 \times \frac{1}{2} \times \frac{1}{2}$	42.5	98
Example 3 C222 2591 unique data a = 11.20, b = 11.70, c = 26.05				
ALF	30 x 30 x 62	$1 \times \frac{1}{2} \times \frac{1}{2}$	442.3	108
		$1 \times 1 \times \frac{1}{2}$	620.0	108
ALFF	32 x 32 x 64	$1 \times \frac{1}{2} \times \frac{1}{2}$	30.5	98
		$1 \times 1 \times \frac{1}{2}$	32.5	98
Example 4 $P6_3/mmc$ 289 unique data a = 9.59, c = 22.67				
HEX	30 x 30 x 64	$1 \times 1 \times \frac{1}{2}$	49.5	70
ALFF	32 x 32 x 64	$1 \times 1 \times \frac{1}{2}$	27.8	98

The four examples compared in Table 14 were selected as representative problems currently being studied in this laboratory. The disparity in the number of grid points is due to restrictions of the particular algorithm (axis length = 2^m in ALFF and = 4n + 2 in ALF and HEX). The CPU time for required prior steps such as equivalent data generation and data sorting was typically 5 sec for ALF and HEX and 10 sec for ALFF.

The examples clearly demonstrate that the FF algorithm is far superior to the TF algorithm. Table 15 summarizes these results in terms of the TF to FF CPU time ratios, and the number of grid points to number of data ratios (symmetry equivalent data are included in the number of data). These data emphasize the fact that the time ratio TF:FF increases dramatically as the total number of data approaches the number of grid points.

Table 15. Comparison of Fourier algorithms

Example	CPU time ratio (TF/FF)	Grid points/data ratio
1	4.7	4.5
2	7.6	5.3
3	14.1 (1/4 map) 19.0 (1/2 map)	3.35
4	1.8	13.0

Example 4 is particularly important since HEX was written for a specific problem. To reduce CPU time, this program was written in FORTRAN and compiled with maximum possible optimization; also specific use of space group symmetry and use of fixed axial lengths were included. The large ratio of grid points to data strongly favors the TF algorithm. However, the FF algorithm was 1.8 times faster in this extreme comparison.[†]

The execution time of ALFF depends mainly on the number of grid points and only weakly on the number of data. Figure 8 shows that the overall time dependence is linear if plotted against $N\log_2 N$ where N equals the total number of grid points. The data used in Figure 1 were collected from a number of different problems in which full maps were calculated and the results printed. In comparison the TF time dependence is a complicated function (very approximately $N^{4/3}$). Thus the TF algorithm (compared to the FF algorithm) becomes increasingly less efficient as N increases.

The FF algorithm as it is typically implemented, has one restriction. Each axis length must be 2^m where m is an integer. However, this was found to be a very minor consideration since much faster computer turnaround and

---

[†] An additional comparison has recently been provided by Dr. Banaszak.[69] In his study of a large biological problem, ALFF was a factor of two faster than the previously used FORTRAN program. In addition, ALFF required considerably less core storage.

Figure 8. $N\log_2 N$ vs. time for the fast Fourier algorithm

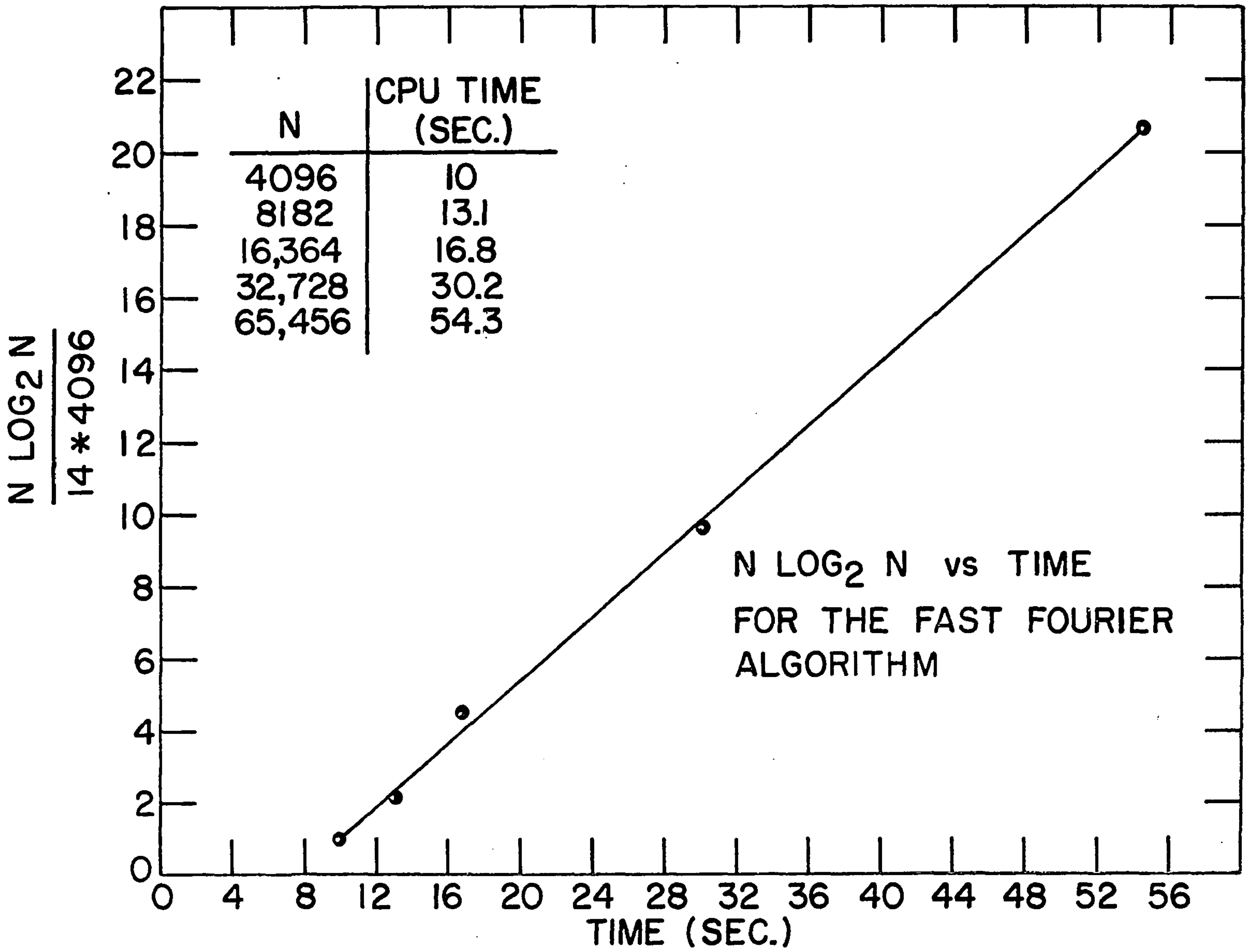

N	CPU TIME (SEC.)
4096	10
8182	13.1
16,364	16.8
32,728	30.2
65,456	54.3

significant reduction in computer time are obtained. Fast Fourier algorithms have been reported for general axis lengths.[65] However, the increased generality introduces a corresponding loss in efficiency. The rapid calculation of Fourier series has enabled new techniques of crystal structure determination to be investigated. However, it is clear that investigators in all areas of crystallography can benefit from the use of the FF algorithm, particularly now with emphasis shifting to the structure determination of large molecules.

Other Programs

The three programs WILSON, SHARP and HPR were written to provide calculation of a Wilson plot,[70] data sharpening[71] and the Howells, Phillips and Rogers[33] statistical test. All three programs were written in FORTRAN IV for the IBM 360/65 computer. The data sets required by these programs are identical for ease of use.

The analysis of white radiation data necessitated a major revision of ORFLS.[13] The resulting white radiation least-squares program WIRALS refines the structural model, extinction parameters, flux parameters and a scale factor. The refinement is based on the observed and calculated intensities. All observations, including those with $I_{obs} < 0.0$, can be included in the refinement. The program also includes correction of calculated intensities for absorption and Lorentz factors.

SUPERPOSITION PHASING USING FOURIER TRANSFORM COEFFICIENTS FROM SUPERPOSITION MAPS

Introduction

The phase problem is commonly solved by heavy atom phasing,[72] Patterson deconvolution[55] or direct methods.[54] The first two are basically real space methods which permit the crystallographer to employ his knowledge of chemistry. Direct methods can not effectively use any chemical information in the very important initial stages due to the methods' statistical basis.[73] The Patterson deconvolution method has been greatly extended thru use of symmetry maps,[56,57] frequency maps[74] and the discriminator index.[61] When a fragment of a structure is known, Karle[75] has shown that a partial set of phases can be derived by assigning the phase of F_{calc} to $|F_{obs}|$ when both $|F_{calc}|$ and $|F_{obs}|$ satisfy certain criteria. The tangent formula is then used to expand the starting set of phases. The resulting E-map may reveal the structure or only a larger fragment. In the latter case the process is repeated. Simonov[76] has presented a method in which a Fourier transform of a superposition map leads to phases for $|F_{obs}|$. The phased structure factors are subsequently used to calculate a pseudo electron-density map from which the atom locations are obtained. The results of Simonov's method are quite impressive, although only problems containing heavy atoms were used as test examples. In addition, Simonov, always utilized the special shift vector (2x, 2y, 2z) which, theoretically, should leave only one image of the structure in the superposition map.

The Fourier transformation from real space to reciprocal space has also been applied in two other methods. The self convolution of the superposition map has had limited success in locating the translation vector between images of the structure[77] and in locating symmetry elements[60] in the superposition map. Recently, the extension of low resolution protein phases to higher resolution has been attempted[62] through modifying and transforming a low resolution electron density map. The results, however, were rather inconclusive.

The coupling of the investigator's knowledge with the power of direct methods can possibly make efficient use of the advantages of both the Patterson deconvolution and direct methods. This is the goal of the superposition phasing method described below. The superposition and fast Fourier systems of programs described previously make this method feasible in terms of computational costs.

Outline of the Method

The first step is the calculation of a pseudo electron-density map $M(\underline{r})$ from a Patterson-symmetry or Patterson-Patterson (P-P) superposition as defined in Table 16. In the

Table 16. Basic definitions used in the superposition phasing method

---

Symmetry maps

$$S(\underline{r}) = \{\mathrm{Min}[w_1P(\underline{v}_1),\ w_2P(\underline{v}_2), \ldots\ w_nP(\underline{v}_n)]\}^{1/2}$$

where $\underline{r}$ is a point in real space, $\underline{v}_i$ is the i^{th} symmetry vector between $\underline{r}$ and a symmetry related point $\underline{r}'$ and w_i is the reciprocal of the multiplicity of $\underline{v}_i$.

Superposition maps

$$M(\underline{r}-\underline{s}_o) = \mathrm{Min}[w_oB(\underline{r}),\ w_1P(\underline{r}-\underline{v}_1),\ w_2P(\underline{r}-\underline{v}_2), \ldots]$$

where $B(\underline{r})$ is a Patterson ($w_o = 1/Z$) or a symmetry map ($w_o = 1$), $\underline{v}_i$ is the i^{th} shift vector, w_i equals $1/Z$ and $\underline{s}_o$ is the shift vector such that the origin defined by the symmetry elements is at $\underline{r}-\underline{s}_o = 0$.

Normalized structure factors from a map

$$U(\underline{h}) = \frac{G(h) * e^{B\sin^2\theta/\lambda^2}}{G(\underline{h}=0)}$$

$$E_G^{\,2}(\underline{h}) = \frac{U^2(\underline{h})}{\varepsilon\langle U^2\rangle}$$

P-P case the symmetry elements should be located, and all symmetry related superpositions should be included in the generation of $M(\underline{r})$. In addition, $M(\underline{r})$ should be modified such that the origin defined by the symmetry elements lies at $\underline{r} = 0$. Next the Fourier transform coefficients $G(\underline{h})$ are calculated from $M(\underline{r})$ by

$$G(\underline{h}) = \int_V M(\underline{r})\, e^{2\pi i \underline{h}\cdot\underline{r}}\, dV. \qquad (22)$$

The phased structure factors from $M(\underline{r})$ are sharpened and converted to normalized structure factors $E_G(\underline{h})$. Normalized structure factors are used to eliminate the $\sin(\theta)/\lambda$ dependence and to allow for normalization of all classes of reflections to a common basis. Finally the phase of $E_G(\underline{h})$ is assigned to $|E_F(\underline{h})|$ when the following conditions are satisfied:

$$|E_G(\underline{h})| \geq \bar{\bar{E}}_G \qquad \text{and} \qquad |E_F(\underline{h})| \geq \bar{\bar{E}}_F \qquad (23)$$

where $\bar{\bar{E}}_G$ and $\bar{\bar{E}}_F$ are adjustable limits. The phased E_F's can then be used to directly calculate an E-map or used in a technique similar to Karle's method of expansion of phases obtained from a fragment. In the latter case the limited set of phased E_F's should be a good starting set for this direct method.

Justification of the Method

A rigorous discussion of the superposition phasing method is impossible since a number of assumptions must be introduced to describe $M(\underline{r})$. The description of $M(\underline{r})$ presented below is quite reasonable and the subsequent equations indicate the validity of the superposition phasing method.

If no errors were introduced in the calculation of $M(\underline{r})$ then this map (consisting of N peaks) contains all S peaks of the structure and N-S accidental peaks. Each peak is assumed to represent a weighted pseudo electron-density distribution. The peaks may overlap forming regions without distinct maxima. Assuming equal atoms the normalized Fourier coefficients $E_G(\underline{h})$ (see Table 16) can be represented as a summation over the N peaks of $M(\underline{r})$:

$$E_G(\underline{h}) \cong \frac{1}{\varepsilon N^{1/2}} \left(\sum_{i=1}^{S} w_i e^{2\pi i \underline{h}\cdot\underline{r}_i} + \sum_{j=1}^{N-S} w_j e^{2\pi i \underline{h}\cdot\underline{r}_j} \right) , \qquad (24)$$

where w_i (≥ 1) is a multiplicity factor necessary to correctly weight the i^{th} peak located at $\underline{r}_i$. The factor ε normalizes all classes of reflections to a common basis.[78]

If all S peaks have weight w then Equation 24 reduces to

$$E_G(\underline{h}) \cong w(S/N)^{1/2} E_F(\underline{h}) + \frac{1}{\varepsilon N^{1/2}} \sum_{j=1}^{N-S} w_j e^{2\pi i \underline{h}\cdot\underline{r}_j} \qquad (25)$$

since $E_F(\underline{h}) = \frac{1}{\varepsilon S^{1/2}} \sum_{i=1}^{S} e^{2\pi i \underline{h}\cdot\underline{r}_i}$. A small correction term could be added to Equation 25 to account for the few peaks with weights unequal to w. However, the magnitude of this correction should be small when $\bar{E}_F$ is large. The summation over all accidental peaks will generally have a value near zero since the vectors $\underline{r}_j$ are randomly oriented. If, accidentally, this summation is large, if N-S is not >>S and if both $|E_G(\underline{h})|$ and $|E_F(\underline{h})|$ are large, then the two terms on the right hand side of Equation 25 must contribute approximately in phase. Therefore Equation 25 indicates that when Equation 23 is satisfied

$$\phi_F(\underline{h}) \cong \phi_G(\underline{h}), \tag{26}$$

where $\phi_G(\underline{h})$ is the phase of $E_G(\underline{h})$ calculated from $M(\underline{r})$ and $\phi_F(\underline{h})$ is the unknown phase.

For example assume $M(\underline{r})$ equals the true electron density function $\rho(\underline{r})$. Obviously, Equation 26 is exact. Now assume that $M(\underline{r})$ contains two complete images of the structure translated by the vector $\underline{t}$ from one another. Since $M(\underline{r}) = \rho(\underline{r}) + \rho(\underline{r} + \underline{t})$ then

$$E_G(\underline{h}) = \frac{1}{\sqrt{2}} E_F(\underline{h}) + \frac{1}{\sqrt{2}} E_F(\underline{h})\, e^{2\pi i \underline{h}\cdot\underline{t}}$$

and (27)

$$|E_G(\underline{h})|^2 = |E_F(\underline{h})|^2 + |E_F(\underline{h})|^2 \cos(2\pi \underline{h}\cdot\underline{t}).$$

When $|E_G(\underline{h})|$ is sufficiently large the term $|E_F(\underline{h})|^2 \cos(2\pi\underline{h}\cdot\underline{t})$ must $\simeq |E_F(\underline{h})|^2$. However, when $2\pi\,\underline{h}\cdot\underline{t} \neq 0$ then $|E_G|^2$ is reduced in magnitude. Thus the condition that $|E_G(\underline{h})| \geq \bar{E}_G$ is important to insure that the phase $\Phi_G(\underline{h})$ is close to $\Phi_F(\underline{h})$.

The above arguments indicate that Equation 26 will hold with greater likelihood for larger $\bar{E}_F$ and $\bar{E}_G$. If direct methods are to be used, the limits should be relatively large since an incorrectly phased E would complicate and/or prevent the success of direct methods. The starting set can be checked for consistency using the tangent formula. Inconsistent phases are suspect and should be omitted from the basis set. If an E-map is to be calculated directly, then lower limits may be acceptable.

Examples

Three known centric structures have been solved using the superposition phasing method. Each of these structures was previously determined using one or more of the basic phasing techniques. The results are presented below and are summarized in Table 17.

π-$C_5H_5Mn(CO)_3$

The structure of π-cyclopentadienyl manganese tricarbonyl was determined[79] using the heavy atom phasing method. A Patterson-symmetry superposition map was calculated using the

Table 17. Direct phasing examples

Compound	$C_5H_5Mn(CO)_3$	$C_4H_4O_3$		$C_{16}H_{18}N_2O_6$
Space group	$P2_1/c$	Pnma		$P2_1/c$
Z	4	4		2
$\bar{E}_F$	1.0	1.25		2.0
$\bar{E}_G$	0.75	1.0		1.25
Superpositions	4	8	4	8
Phases predicted	191	32	29	24
Phases correct	191	32	23	24

Mn positions as shift vectors. The superposition phasing method correctly signed all 191 structure factors which satisfied Equation 23 with $\bar{E}_F = 1.0$ and $\bar{E}_G = 0.75$. The pseudo symmetry found in the heavy atom solution also existed in the E-map calculated from the 191 signed normalized structure factors. However, the structure was easily identified in this map.

$C_4H_4O_3$

The structure of tetrahydro-3,4-furandione was solved[80] by use of trial and error superposition techniques. The structure has subsequently been solved testing both direct and Patterson-symmetry map superposition methods. A resolved peak in the symmetry map was selected, and the Patterson-symmetry map superposition was calculated using the location of this peak and the seven symmetry related peaks for shift vectors. The only assumption involved is that the choosen peak is at a real atom location. With limits of $\bar{E}_F = 1.25$ and $\bar{E}_G = 1.0$, 32 structure factors were signed without error. These 32 signed structure factors were then used as a starting set for direct methods using the Σ_2 relation.[73] No symbols were introduced during the application of the Σ_2 relation. An additional 27 signs were determined for structure factors with $|E(\underline{h})| \geq 1.0$. These 59 signed E's were sufficient for calculation of a clear E-map which contained peaks only at atomic positions.

$C_{16}H_{18}N_2O_6$

The structure of β-picoline-N-oxide fumaric acid adduct was solved[81] using a combination of Patterson-symmetry map superposition, frequency checks and chemical knowledge. Direct methods were unable to solve this structure. The Patterson and symmetry maps had very dense planes as the molecule is essentially planar. A partially resolved peak in the symmetry map was found and the four symmetry related shift vectors were used to calculate M($\underline{r}$). This map was still quite dense. A second peak was found 1.5 Å, an expected C-C bond distance, from the first in M($\underline{r}$). Using this second peak and the three symmetry related peaks, four additional superpositions were calculated to reduce the number of accidental peaks. Using the Fourier coefficients from this second map all 24 predicted signs were correct. This initial set of phased E's was then used as a starting set for direct methods. However, it was necessary to introduce two arbitrary symbols before a sufficient number of large E's were signed. The resultant E-map contained peaks at the location of all atoms of the structure plus about 50% extra peaks. The extraneous peaks were generally weaker than true peaks and a model clearly revealed the true structure.

Discussion

The use of Fourier transform coefficients from superposition maps for phasing of structure factors is a powerful extension of Patterson deconvolution methods. Since chemical and symmetry knowledge can be easily included, this method can be very powerful when coupled with direct methods. This method should also be applicable to acentric structures, particularily since the initial step of forming the superposition map is independent of a center of symmetry. However, initial tests on an acentric structure have not been entirely successful.

Heavy atom structures can easily be solved using the superposition phasing technique; problems with a small Z^2 ratio[72] may be more readily solved using this method instead of the heavy atom approach. For heavy atom problems such as π-cyclopentadienyl manganese tricarbonyl the superposition phasing method can lead directly to an electron density map.

The basic problem of selecting numerous consistent shift vectors in the Patterson deconvolution method is reduced; only a limited number of superpositions are required before transforming to reciprocal space. In two of the three test structures studied only the minimum number of symmetry related superpositions were used to form $M(\underline{r})$. The limitations of this method are connected to the limitations of Patterson deconvolution methods. The number of accidental peaks in $M(\underline{r})$ must not be too large; the peaks of the structure should be a significant fraction of the total number of peaks. In addition, higher symmetry structures, e.g. orthorhombic, are easier to solve using Patterson-symmetry map superpositions to form $M(\underline{r})$ than are triclinic structures where more symmetry independent shift vectors must be used to reduce to N images of the Patterson to approximately one image.

The determination of a sizeable starting set of phases for direct methods is very important. This set may be sufficiently large such that no symbols need to be introduced in the application of the Σ_2 relation. In addition the difficulty of selecting a good set of origin determining reflections is eliminated. The success of this method for centric problems reveals that the Fourier coefficients from superposition maps do indeed contain a great deal of information about the structure.

REFERENCES

1. S. L. Lawton and R. A. Jacobson, J. Amer. Chem. Soc. 88, 616 (1966).

2. P. Day, Inorg. Chem. 2, 452 (1963).

3. S. L. Lawton, R. A. Jacobson and R. S. Frye, Inorg. Chem. 10, 701 (1971).

4. S. L. Lawton and R. A. Jacobson, Inorg. Chem. 7, 2124 (1968).

5. M. L. Hackert, S. L. Lawton and R. A. Jacobson, Iowa Academy of Science 75, 97 (1968).

6. F. Ephraim and S. Weinberg, Ber. Deut. Chem. Ges. 42, 4447 (1909).

7. A. T. Jensen and S. E. Rasmussen, Acta Chem. Scand. 9, 708 (1955).

8. D. E. Williams, AEC Report IS-1052, Ames Laboratory, Ames, Iowa, 1964.

9. Several undocumented programs written at Ames Laboratory, Ames, Iowa by D. E. Williams, R. K. Wismer and others were used for some calculations reported in this text.

10. L. E. Alexander and G. S. Smith, Acta Cryst. 15, 983 (1962).

11. D. E. Williams and R. E. Rundle, J. Amer. Chem. Soc. 86, 1660 (1964).

12. D. J. Wehe, W. R. Busing and H. A. Levy, AEC Report ORNL-TM-299, Oak Ridge National Laboratory, Oak Ridge, Tennessee, 1962.

13. W. R. Busing, K. O. Martin and H. A. Levy, AEC Report ORNL-TM-305, Oak Ridge National Laboratory, Oak Ridge, Tennessee, 1962.

14. H. P. Hanson, F. Herman, J. D. Lea and S. Skellman, Acta Cryst. 17, 1040 (1964).

15. D. H. Templeton in "International Tables for X-ray Crystallography," Vol. III, The Kynock Press, Birmingham, England, 1962, pp. 215, 216, Table 3.3.2C.

16. C. J. Fritchie in "Proc. of the Symposium on X-ray Intensity Measurement," Trans. Amer. Cryst. Assn. 1, p 30 (1965).

17. W. R. Busing, K. O. Martin and H. A. Levy, AEC Report ORNL-TM-306, Oak Ridge National Laboratory, Oak Ridge, Tennessee, 1964.

18. C. K. Johnson, AEC Report ORNL-3794, Oak Ridge National Laboratory, Oak Ridge, Tennessee, 1965.

19. A. F. Wells, "Structural Inorganic Chemistry," 3rd ed, Oxford Clarendon Press, London, England, 1962, p 172.

20. L. Pauling, "The Nature of the Chemical Bond," 3rd ed, Cornell University Press, Ithaca, New York, 1960, p 514.

21. D. S. Urch, J. Chem. Soc. Suppl. 1, 5775 (1964).

22. C. R. Hubbard and R. A. Jacobson, Iowa Academy of Science 75, 85 (1968).

23. S. K. Porter and R. A. Jacobson, J. Chem. Soc. Sect. A, 1359 (1970).

24. S. K. Porter and R. A. Jacobson, J. Chem. Soc. Sect. A, 1356 (1970).

25. J. R. Clark, R. A. Jacobson and R. G. Baughman, Iowa State Univ., personal communication, 1971.

26. M. L. Hackert, R. A. Jacobson and T. A. Keiderling, Inorg. Chem. 10, 1075 (1971).

27. S. L. Lawton and R. A. Jacobson, Inorg. Chem. 10, 709 (1971).

28. A. Rosenheim and W. Stellman, Ber. Chem. Dtsh. Ges. 34, 3377 (1901).

29. R. D. Whealy and R. L. Yeakley, J. Inorg. Nucl. Chem. 25, 365 (1963).

30. G. C. Allen and N. S. Hush, Prog. in Inorg. Chem. 8, 357 (1967).

31. W. Petzold, Z. Anorg. Allg. Chem. 215, 92 (1933).

32. W. R. Busing and H. A. Levy, Acta Cryst. 10, 180 (1967).

33. E. R. Howells, D. C. Phillips and D. Rogers, Acta Cryst. 3, 210 (1950).

34. D. T. Cromer and J. T. Waber, Acta Cryst. 18, 104 (1965).

35. B. Vonnegut and B. E. Warren, J. Amer. Chem. Soc. 58, 2459 (1936).

36. L. Pauling, "The Nature of the Chemical Bond," 3rd ed, Cornell Univ. Press, Ithaca, New York, 1960, p 260.

37. G. L. Breneman and R. D. Willett, Acta Cryst. 23, 467 (1967).

38. J. F. Colwell, P. H. Miller and W. L. Whittemore in "Neutron Inelastic Scattering," Vol. II, International Atomic Energy Agency, Vienna, Austria, 1968, pp 429-437.

39. F. Gompf, W. Reichardt, W. Glaser and K. H. Beckurts in "Neutron Inelastic Scattering," Vol. II, International Atomic Energy Agency, Vienna, Austria, 1968, pp 417-428.

40. R. D. Lowde, Acta Cryst. 9, 151 (1956).

41. R. D. Lowde, Nature 167, 243 (1951).

42. B. Buras, T. Giebultowiez, W. Minor and A. Rajca, Nuclear Instr. Meth. 77, 13 (1970).

43. W. H. Zachariasen, Acta Cryst. 23, 558 (1967).

44. W. H. Zachariasen, Acta Cryst. A24, pp 212, 324, 425 (1968).

45. E. Melkonian, Phys. Rev. 76, 1750 (1949).

46. G. E. Bacon and J. Thewlis, Proc. Roy. Soc. A. 196, 50 (1949).

47. B. Lebech and K. Mikke, Riso Report No. 164, Danish Atomic Energy Commission, Riso, Roskilde, Denmark, 1967.

48. G. E. Bacon, "Neutron Diffraction," Oxford Press, London, England, 1962, pp 31, 61.

49. Neutron Diffraction Commission, Acta Cryst. A25, 391 (1969).

50. W. J. L. Buyers and T. Smith, J. Phys. Chem. Solids 29, 1051 (1968).

51. T. M. Sabine, G. W. Cox and B. M. Craven, Acta Cryst. B25, 2437 (1969).

52. R. G. Delaplane and J. A. Ibers, Acta Cryst. B25, 2423 (1969).

53. L. M. Corliss, J. M. Hastings and R. J. Weiss, Phys. Rev. Letters 3, 211 (1959).

54. F. R. Ahmed, Ed., "Crystallographic Computing," Munksgaard, Copenhagen, Denmark, 1970.

55. M. J. Buerger, "Vector Space," John Wiley and Sons, Inc., New York, New York, 1959.

56. A. D. Mighell and R. A. Jacobson, Acta Cryst. 16, 443 (1963).

57. P. G. Simpson, R. D. Dobrott and W. N. Lipscomb, Acta Cryst. 18, 169 (1965).

58. J. Rodgers and R. A. Jacobson, AEC Report IS-2155, Ames Laboratory, Ames, Iowa, 1969.

59. C. R. Hubbard and R. A. Jacobson, AEC Report IS-2210, Ames, Laboratory, Ames, Iowa, 1969.

60. C. R. Hubbard and R. A. Jacobson, Abstracts, 1970 Winter Amer. Cryst. Assoc. Meeting, Tulane University, March 1970, Paper B1.

61. M. L. Hackert and R. A. Jacobson, Acta Cryst. B26, 1682 (1971).

62. A. N. Barrett and M. Zwick, Acta Cryst. A27, 6 (1971).

63. J. W. Cooley and J. W. Tukey, Math. of Computation 19, No. 90, p 297.

64. W. M. Gentleman and G. Sande, Proceedings - Fall Joint Computer Conference, 1966, p 563 (1966).

65. G. D. Bergland, IEEE Spectrum, p 41, July 1969.

66. A. L. Patterson in "International Tables for X-ray Crystallography," Vol. II, The Kynock Press, Birmingham, England, p 78, 1962.

67. C. R. Hubbard, C. O. Quicksall and R. A. Jacobson, AEC Report IS-2625, Ames Laboratory, Ames, Iowa, 1971.

68. "PL/1 Scientific Subroutine Package," IBM Manual H20-0544-1, IBM, White Plains, New York, 1968, p 134.

69. L. Banaszak, Washington University of St. Louis, personal communication, 1971.

70. G. H. Stout and L. H. Jensen, "X-ray Structure Determination," The Macmillan Company, New York, New York, 1968, p 205.

71. R. A. Jacobson, J. A. Wunderlick and W. N. Lipscomb, Acta Cryst. 14, 598 (1961).

72. H. S. Lipson and W. Cochran, "The Determination of Crystal Structures," Bell, London, 1953.

73. H. Hauptman and J. Karle, "Solution of the Phase Problem. I. The Centrosymmetric Crystal," A.C.A. Monograph No. 3, Polycrystal Book Service, Pittsburg, 1953.

74. B. T. Gorres and R. A. Jacobson, Acta Cryst. 17, 1599 (1964).

75. J. Karle in "Crystallographic Computing," F. R. Ahmed, Ed., Munksgaard, Copenhagen, Denmark, 1970, p 37.

76. V. I. Simonov, Acta Cryst. B25, 1 (1969).

77. G. Germain and M. M. Woolfson, Acta Cryst. 21, 845 (1966).

78. A. J. C. Wilson, Acta Cryst. 17, 1591 (1964).

79. A. F. Berndt and R. E. Marsh, Acta Cryst. 16, 118 (1963).

80. F. A. Muller, Ph.D. Thesis, Princeton University, Princeton, New Jersey, 1964.

81. B. T. Gorres, Ph.D. Thesis, Princeton University, Princeton, New Jersey, 1964.

ACKNOWLEDGEMENTS

For helping to make his graduate study at Iowa State University a rewarding experience, the author wishes to express his sincere appreciation to:

Prof. Robert A. Jacobson for his inspiration, continued guidance and helpful discussions concerning this work;

Dr. C. O. Quicksall, whose assistance and critical advice was very important throughout the development of both the white radiation technique and the fast Fourier programs;

the State of Iowa and the United States government for financial support in the form of teaching and research assistantships, an NSF traineeship and an NSF travel grant to attend the NATO Advance Studies Institute on Direct and Patterson Methods;

Mr. J. E. Benson and Mr. J. R. Clark for their assistance with automation of the Datex diffractometer and for their day to day assistance with the research equipment;

and my wife, Jayne, for her loving patience and understanding during the last four years.